Estropausal gut microbiota transplant improves ovarian function in adult mice

Minhoo Kim[1], Justin Wang[1,2,3], Ryan J. Lu[1,4], Younggyun Kim[1,5], Minying Liu[6], Xueyan Fu[6], Sarah L. Booth[6] and Bérénice A. Benayoun[1,7,8,9,10]

1. Leonard Davis School of Gerontology, University of Southern California, Los Angeles, CA 90089, USA.
2. Department of Quantitative and Computational Biology, University of Southern California, Los Angeles, CA 90089, USA.
3. Department of Chemistry, University of Southern California, Los Angeles, CA 90089, USA.
4. Graduate Program in the Biology of Aging, University of Southern California, Los Angeles, CA 90089, USA.
5. Alfred E. Mann Department of Biomedical Engineering, University of Southern California, Los Angeles, CA 90089, USA.
6. Jean Mayer USDA Human Nutrition Research Center on Aging at Tufts University, Boston, MA 02111, USA
7. Molecular and Computational Biology Department, USC Dornsife College of Letters, Arts and Sciences, Los Angeles, CA 90089, USA.
8. Biochemistry and Molecular Medicine Department, USC Keck School of Medicine, Los Angeles, CA 90089, USA.
9. USC Norris Comprehensive Cancer Center, Epigenetics and Gene Regulation, Los Angeles, CA 90089, USA.
10. USC Stem Cell Initiative, Los Angeles, CA 90089, USA.

*Correspondence: berenice.benayoun@usc.edu

Summary

Decline in ovarian function with age not only affects fertility but is also linked to a higher risk of age-related diseases in women (*e.g*. osteoporosis, dementia). Intriguingly, earlier menopause is linked to shorter lifespan; however, the underlying molecular mechanisms of ovarian aging are not well understood. Recent evidence suggests the gut microbiota may influence ovarian health. In this study, we investigated the effect of the gut microbiome from young and estropausal female mice on ovarian health through fecal microbiota transplantation. We demonstrate that the ovarian transcriptome can be broadly remodeled after heterochronic microbiota transplantation, with a reduction in inflammation-related gene expression and trends consistent with transcriptional rejuvenation. Consistently, these mice exhibited enhanced ovarian health and increased fertility. We also identified candidate microbial genera potentially responsible for the observed transcriptomic changes through causal mediation analyses. Our findings reveal a direct link between the gut microbiota and ovarian health.

Keywords

Microbiome, ovarian aging, menopause, 16S amplicon sequencing, ovarian RNA-seq

Introduction

Women are born with a definitive number of ovarian follicles and the gradual decrease in the number of the follicles ultimately leads to menopause[1-3]. The onset of menopause has been linked with an elevated risk of numerous age-related conditions, including osteoporosis and dementia[4-6]. Moreover, a later onset of menopause has been identified as a potential predictor of extended lifespan[7,8]. While the profound effects of menopause on the health- and lifespan of women are well-documented, the factors that contribute to ovarian aging and the strategies for its prevention remain poorly understood.

During the reproductive years, the hypothalamus-pituitary-ovarian hormone axis ensures the proper production and release of hormones necessary for ovulation and menstruation[9]. However, as menopause progresses, ovaries become less responsive due to reduced follicle numbers, ultimately leading to the hormonal imbalances characteristic of menopause[10]. Specifically, the serum concentrations of follicle-stimulating hormone (FSH) and luteinizing hormone (LH) increase, whereas anti-Müllerian hormone (AMH) and Inhibin A (INHBA) decrease with menopause progression[11-13]. These hormonal adjustments are hallmarks of the menopausal transition and highlight the diminished function of the ovaries[10]. Importantly, this disrupted feedback mechanism has been attributed to the wide array of menopausal symptoms and health risks associated with this transition phase[14,15]. For instance, recent studies have shown FSH receptor activation by FSH in the brain increases susceptibility for Alzheimer's disease pathogenesis in women and blockade of FSH improves cognition in a mouse model of Alzheimer's disease[14,16].

The adult human gut microbiome is composed of approximately 10^{13} to 10^{14} micro-organisms[17,18]. The microbiome consists of bacteria, viruses and fungi, with bacteria representing the largest proportion of the microbial population[19]. Perturbations in the gut microbiota configuration are reported to lead to development and/or progression of serious disease, including diabetes and depression[20,21]. Interestingly, reported health effects of fecal microbiota derived from aged individuals have been inconsistent[22,23]. For example, one study demonstrated that fecal microbiota transplantation (FMT) from 24-month-old mice to 3-month-old mice led to the acceleration of age-associated phenotypes in the brain, retina, and gut of the recipient mice[22]. In contrast, another study found that grafting of fecal microbiota from 24-month-old mice to 5- to 6-week-old germ-free mice enhanced neurogenesis in the hippocampus and induced intestinal

growth[23]. These findings underscore the microbiome's complex, multifaceted effects on various organ systems throughout life, significantly affecting host health.

A recent study discovered that women with premature ovarian insufficiency exhibited significantly altered gut microbial profiles compared to healthy women[24]. Notably, alternations in the gut microbiome in premature ovarian insufficiency patients were associated with changes in serum hormone levels of key ovarian endocrine markers, including FSH, LH and AMH[24]. Similarly, the composition of the gut microbiome has been implicated in the development of polycystic ovary syndrome (PCOS), a disorder characterized by hyperandrogenism and polycystic ovaries[25]. Specifically, FMT of samples from PCOS patients to mice resulted in ovarian dysfunction in otherwise healthy recipient mice[25]. Consistent with the importance of a healthy microbiome for ovarian function, another study has shown that 17β-estradiol levels are significantly lowered in the germ-free female mice[26]. Moreover, transcriptome analysis of sexual development marker genes of the liver and histological studies of ovarian follicle development in germ-free female mice indicated that sexual maturation is perturbed in microbiota-depleted mice[26]. Importantly, the gut microbiota has been shown to modulate serum estrogen levels (through the “estrobolome”), further highlighting the potential role of the gut microbiota in female reproductive health[27]. The gut microbiota regulates action of estrogens through the secretion of β-glucuronidase, an enzyme that deconjugates estrogens into their active forms[27-29]. Dysbiosis of the gut microbiota can impair this process, leading to a reduction in circulating estrogens and potentially contributing to the development of estrogen-modulated conditions[27]. Collectively, these findings highlight a significant causal relationship between the gut microbiota and ovarian function and health, suggesting a pivotal role for microbial communities in modulating female reproductive conditions.

In this study, we analyzed the gut microbial profiles of young and estropausal (post-reproductive phase in rodents, analogous to human menopause) female mice via 16S rRNA amplicon sequencing and explored how the distinct microbial communities affect ovarian health through FMT experiments in young female mice. Unbiased RNA-seq analyses revealed that modifying the gut microbiota leads to profound changes in the ovarian transcriptomic landscape. Surprisingly, heterochronic gut microbiota transplant from estropausal mice to young female recipients led to a reduction in inflammation-related gene expression in the ovaries, and dampened expression of genes that tend to be upregulated in aging

ovaries. Consistently, we observed improved ovarian function and health in the estropausal FMT recipients, supporting a surprising finding whereby old gut microbiota has beneficial effects on ovarian health. Lastly, we identified specific microbial genera that might drive the observed transcriptomic changes in the ovaries via causal mediation analyses. Overall, our study shows that manipulating the gut microbiota can directly influence ovarian function and health.

Results

Young and estropausal female mice show distinct fecal microbial profiles

To investigate the potential link between changes in the gut microbiome and ovarian aging in mice, we assessed (1) the ovarian health state and (2) microbial profiles of young (4-months) and naturally aged estropausal (20-months) C57BL/6JNia female mice[30] (Figure 1A). To quantify the overall ovarian health state of the mice, we decided to construct a composite "ovarian health index", similar to the concept of frailty index[31]. This index is designed to provide a comprehensive and integrated evaluation of ovarian function based on the ovarian follicle reserve and the serum concentrations of critical pituitary and ovarian hormones: AMH, FSH, and Inhibin A (Figures 1A and B; see methods). Consistent with previous reports[30,32], we observed a significant reduction in ovarian follicle counts and serum levels of AMH and Inhibin A, as well as increased FSH levels in the estropausal group (Figures S1A-D). Furthermore, the estropausal group exhibited a significantly lower ovarian health index score compared to the young group (p-value ~0.0109; Figure 1B), validating the subsequent use of our index as a measure of ovarian health and function.

We then collected fecal samples from four independent cohorts of mice and performed 16S rRNA V3-V4 amplicon sequencing to compare the gut microbial profiles of the young and estropausal female mice. 16S rRNA amplicon sequencing allows identification of bacteria at the genus level by amplifying and sequencing variable regions of the 16S rRNA gene (*e.g.* V3-V4 region), which contains unique sequences specific to different species[33]. Quantification and analysis of the sequences from the variable regions, or amplicon sequence variants (ASVs), have been shown to provide important insights of the microbial compositions and environment[34].

Our analysis focused on both beta diversity, which assesses differences between microbial communities, and alpha diversity, which looks at diversity within a community[35,36]. Beta diversity was evaluated using the Bray-Curtis dissimilarity and Jaccard index (Figures S1E). The analysis of Bray-Curtis dissimilarity and Jaccard index, conducted by cohort, revealed a distinct separation between the young and estropausal female groups (Figure S1E). Moreover, the results of the principal component analysis, applied to center log-ratio (CLR)-transformed and batch-corrected ASV counts, further highlighted clear clustering between the young and estropausal females across 4 independent cohorts of animals (Figure

1C). Alpha diversity measures the diversity within a single microbial community or ecosystem, focusing on the variety and abundance of ASVs in a specific environment[36]. We evaluated alpha diversity through four indices: Observed features, Evenness Pielou, Shannon entropy, and Faith's Phylogenetic Diversity (Faith PD). Importantly, estropausal females exhibited significantly higher scores in all four indices compared to the young female group (Figure 1D). Our results suggest that the estropausal females have a higher biodiversity, indicated by a larger number of observed features; a more uniform distribution of ASV abundances; increased species richness and evenness; and a broader range of genetically diverse species. This pattern of increased alpha diversity with age aligns with findings from human studies[37,38]. Additionally, a recent study reported elevated alpha diversity indices in PCOS model mice[39].

We next asked which specific microbial genera changed in abundance between young and estropausal female mice recurrently across our 4 independent cohorts (Figure 1E). Our analysis identified three genera that were more abundant ("UP in EF") and six that were less abundant ("DOWN in EF") in the microbiota of estropausal females (Figure 1E; absolute effect size > 1, adjusted p-value < 0.05). Most of the differentially abundant genera belonged to the *Lachnospiraceae* family, offering a potential lead for future research on their impact on ovarian health. Previous studies have reported a relative decrease in abundance of microbial species from the *Lachnospiraceae* family with age in humans[40,41]. Further studies will be required to elucidate the molecular mechanisms through which these genera affect ovarian function and health. Additionally, we conducted a predictive analysis of functional consequences of these changes in microbial abundances using PICRUSt2[42] (Figure 1F). This analysis suggested an increase in metabolic pathways such as ketogluconate metabolism and the superpathway of glycerol degradation to 1,3-propanediol, while pathways including the superpathway of fatty acid biosynthesis initiation and phospholipases were predicted to decrease in the estropausal group (Figure 1F). These predicted metabolic changes, including an increase in ketoglutarate and alterations in lipid metabolism, have been previously associated with ovarian cancers, underscoring the potential relevance of our findings to understanding ovarian health[43,44]. Our results collectively underscore the pronounced differences in the fecal microbial profiles between young and estropausal females.

Chemically-induced premature ovarian failure model mice show distinct fecal microbial profiles

The 4-VinylCyclohexene Diepoxide (VCD)-injected mouse model is a follicle-deplete, ovary-intact animal model that is known to recapitulate many key aspects of human ovarian aging[45,46]. VCD accelerates atresia by causing selective loss of primary and primordial follicles in the ovary, while leaving the rest of the ovarian structure intact for residual hormone production[45,46]. We assessed the ovarian health index and fecal microbial profiles of vehicle- and VCD-exposed mice (CTL and VCD, respectively; Figure S2A). Briefly, 4-month-old C57BL/6Tac female mice were subjected to daily treatments of either vehicle (safflower oil) or VCD (at a dosage of 160 mg/kg/day) for 15 consecutive days. Then, the mice were maintained for an additional 100 days to ensure the complete development of phenotypes associated with VCD exposure[47] (Figure S2A). Ovarian follicle depletion and alterations in crucial ovarian hormone levels (*i.e.* AMH, FSH, and Inhibin A) were confirmed through ovarian histology analysis and serum hormone concentration measurements, respectively (Figures S2C-F). In line with these findings, the VCD-treated group exhibited a markedly lower ovarian health index (p-value ~0.0100; Figure S2B), consistent with overall depleted ovarian function.

Subsequently, we conducted 16S rRNA V3-V4 amplicon sequencing on vehicle- and VCD-treated animals. Analysis through principal component analysis of CLR-transformed ASV counts, along with Bray-Curtis dissimilarity and Jaccard index, demonstrated a distinct separation between the vehicle-treated (CTL) and VCD-exposed groups (Figures S3A-B). Alpha diversity indices, on the other hand, revealed no significant differences between these two groups (Figures S3C). These findings suggest that the overall diversity within the group's communities may appear similar, but they may be different in the species present, their relative abundances and the functions the species perform. Indeed, our analysis revealed differentially abundant genera from CTL vs. VCD groups (Figure S3D; absolute effect size > 1, adjusted p-value < 0.05). We detected several genera from the *Lachnospiraceae* family, yet none of the unique ASV IDs corresponded with those identified as differentially abundant in the estropausal female mice. Thus, further research to accurately identify the species significant to ovarian aging and health will be important. Then, we utilized PICRUSt2 to predict functional abundance between the CTL and VCD groups (Figure S3E). Notably, we detected down-regulation of the phospholipases pathway in the VCD group, a finding consistent with observations in the estropausal female group (Figures 1F and S3E). Our

findings suggest that physiological ovarian aging and chemically-induced ovarian failure lead to substantially different outcomes on the gut microbiota.

Young and old male mice show distinct fecal microbial profiles

Next, as an important comparison point, we also characterized the fecal microbial profiles of young (4-months) and naturally aged old (20-months) C57BL/JNia male mice (Figure S4A). This comparative study among female and male aging mice, as well as the VCD-exposed mice, aimed to identify differences in microbial profiles attributable to general aging and those specific to ovarian aging. We collected fecal samples from three independent cohorts of mice and performed 16S rRNA V3-V4 amplicon sequencing to compare the gut microbial profiles of the young and old male mice. Analysis using principal component analysis of CLR-transformed ASV counts, coupled with Bray-Curtis dissimilarity and Jaccard index, showed a distinct divergence between the young and old male groups (Figures S4B-C). However, this separation was less pronounced compared to what was observed in the female cohorts (Figure 1C). Alpha diversity indices indicated no significant disparities between the two age groups of males (Figure S4D). Similarly, a previous study examining microbial profiles in male mice aged 3-4 months and 19-20 months found comparable alpha diversity index values between the two age groups[48]. Through differential abundance and functional abundance prediction analyses, we identified several genera and functional terms that varied significantly between young and old male mice (Figures S4E-F). Importantly, we observed a few consistent functional terms across female and male aging cohorts. In particular, the L-lysine biosynthesis I pathway was found to be up-regulated, while the pyridoxal 5-phosphate biosynthesis I pathway and the superpathway of pyridoxal 5-phosphate biosynthesis were down-regulated with age in both sexes (Figures 1F and S4F). These results suggest that these pathways may play roles in the general aging processes, rather than being uniquely related to ovarian aging. Further research will be necessary to elucidate the influence of these functional pathways on the aging process.

Gut microbiota manipulation can induce changes in the ovarian transcriptome

To investigate the potential effects of gut microbiota on ovarian health, we conducted FMT experiments to directly assess how alterations in the gut microbiota after estropause may influence ovarian function. Specifically, young adult female mice (4-months) were subjected to treatment with anti-biotics/anti-mycotic (Ab/Am) treatment to eliminate their initial microbial environment, and then received fecal microbiota grafts from either young (FMT-YF) or estropausal (FMT-EF) female mice (Figure 2A). Subsequently, the ovaries were harvested for bulk RNA-seq analysis (Figure 2A). Based on previous research that has shown harmful effects of gut microbiota from donors with ovarian dysfunction, such as PCOS[25], our initial hypothesis was that transplanting fecal matter from estropausal mice could potentially induce estropause-like conditions in the recipient mice.

Our multi-dimensional scaling (MDS) analysis of the ovarian RNA-seq dataset revealed a clear separation between the FMT-YF and FMT-EF groups (Figure 2B). Additionally, we detected 2,131 differentially expressed genes between the FMT-YF and FMT-EF groups (FDR < 5%; Figure 2C). Then, we investigated the pathways that were distinctively regulated between the FMT-YF and FMT-EF groups. Our gene set enrichment analysis (GSEA)[49] results highlighted that pathways related to immune regulation were significantly down-regulated in the FMT-EF groups (Figures 2D-F; highlighted in red). To evaluate whether these changes were the results of substantial changes in immune cells infiltration in the tissue, we leveraged a publicly available ovarian single-cell RNA-seq dataset[50] to conduct deconvolution analysis, thus allowing us to deduce alterations in immune cell proportions within our dataset. Using two distinct tools, CSCDRNA[51] and Granulator[52], we determined that the proportions of immune cells did not significantly differ between the FMT-YF and FMT-EF groups (Figure S5A), consistent with the notion that the transcriptional changes that we observed may reflect cell autonomous changes in gene expression profiles.

To identify transcription factors potentially driving the transcriptomic alterations observed between the FMT-YF and FMT-EF groups, we utilized Gene Transcription Regulation Database (GTRD)[53] with the GSEA paradigm. While our analysis did not identify any transcription factors meeting the usual stringent criteria of FDR < 5%, we found two transcription factors showing trends of up-regulation and eight displaying down-regulation trends from the FMT-EF group, with an adjusted FDR < 10% threshold (Figure 2G). Then, we identified publicly available ChIP-seq datasets for the trending transcription factors via the

Cistrome Data Browser[54,55], using corresponding *bona fide* peaks to determine potential enrichment by GSEA. Our analysis showed significant negative enrichment scores of Ncoa1 and Usp7-regulated genes within the FMT-EF group (p-value ~0.0138 and ~1e-04, respectively; Figure S5B). Moreover, we noted that the expression levels of *Ncoa1* and *Usp7* remained consistent across FMT-YF and FMT-EF groups (Figure S5E), suggesting potential post-transcriptional or post-translational regulation. While research on the roles of Ncoa1 and Usp7 in ovarian function is sparse, one study highlighted that Ncoa1 function is important in egg production traits in Shaobo hens[56]. Additionally, an inhibitor of Usp7, P5091, was found to inhibit the proliferation of ovarian cancer cells in another study[57]. Together with our findings, this suggests that Ncoa1 and Usp7 represent potential transcriptional regulators of ovarian function.

Heterochronic FMT may have rejuvenating effects on the ovarian transcriptome of the recipients

Cumulative studies have indicated that aging leads to a pro-inflammatory shift in the ovarian microenvironment, adversely affecting ovarian function and oocyte quality[58,59]. Based on our GSEA results which indicated down-regulation of inflammatory pathways in the ovaries of the FMT-EF group, we next asked whether changes in the ovarian transcriptome upon FMT-EF could represent a more general trend of transcriptional rejuvenation. For this purpose, we analyzed two publicly available bulk RNA-seq datasets profiling ovaries from young (2-3-months) and aged/estropausal (12-months) wild-type female mice[60,61] to identify gene sets that are either up- or down-regulated with ovarian aging (Figure 3A). To evaluate whether the genes identified from publicly available RNA-seq datasets on ovarian aging ("UP with ovarian aging" and "DOWN with ovarian aging") were significantly regulated in response to FMT-EF, we conducted GSEA using significant age-regulated genes as input gene sets. Surprisingly (and contrary to expectations based on previously reported observation at the somatic level for heterochronic FMT), our findings revealed a significant negative enrichment score for genes that were up-regulated in the context of ovarian aging (p-value ~0.0046; Figure 3B), suggesting that the ovarian transcriptome of the heterochronic FMT recipients (*i.e.* FMT-EF group) displays transcriptional profiles resembling those of younger females.

As an orthogonal line of evidence, we next asked whether indicators of cellular senescence (as measured by the highly curated senescent marker gene set, SenMayo[62]) were significantly impacted by

FMT-EF. Importantly, our results showed a significant negative enrichment score for the SenMayo gene set in the FMT-EF group, consistent with an overall “rejuvenation” trend for the ovarian transcriptome of FMT-EF mice (p-value ~0.0382; Figure 3C).

FMT-EF mice show improved ovarian health

Since we observed large ovarian transcriptome remodeling in the FMT-EF group consistent with a less inflammatory, more youthful ovarian state, we next assessed the ovarian health state of the FMT-YF *vs.* FMT-EF groups to determine whether FMT-EF led to enhanced ovarian function (Figure 4). We evaluated ovarian health function using a 2-pronged approach (Figure 4A): (i) calculating the ovarian health index, similarly to the physiological aging and VCD groups (see above, Figures 1B and S2B), and (ii) evaluating effective fertility using litter size and time to first pregnancy after mating[63].

Consistent with our prediction from the ovarian transcriptomes, the FMT-EF mice exhibited significantly higher scores on the composite ovarian health index than FMT-YF mice (p-value ~0.0445; Figures 4B, S6A-D), supporting an enhanced ovarian health phenotype. Next, we evaluated the result of ovarian function – fertility – through measures of litter size and reproductive success rate. Specifically, there was a suggestive trend for increased litter size in FMT-EF mice (p-value ~0.0696; Figure 4C). In addition, FMT-EF mice remained nulliparous for a shorter amount of time after pairing with a young health male (p-value ~0.002; Figure 4D), also suggestive of improved fertility. Together, our findings are consistent with improved/rejuvenated ovarian function after FMT-EF.

FMT-YF and FMT-EF mice show distinct microbial profiles

Importantly, we next verified that fecal transplants from young or estropausal female mice led to distinct microbial profiles in the recipient mice. For this purpose, we conducted and analyzed 16S rRNA V3-V4 amplicon sequencing on the gut microbiota of FMT-YF and FMT-EF mice (Figure 5).

The principal component analysis of CLR-transformed ASV counts, complemented by Bray-Curtis dissimilarity and Jaccard index, showed a clear segregation between the FMT-YF and FMT-EF groups (Figures 5B-C). While no significant differences were noted across four alpha diversity indices (Figures 5D), we identified several microbial genera with significant differential abundance between the FMT-YF

and FMT-EF groups (absolute effect size > 1, adjusted p-value < 0.05; Figure 5E). Notably, two genera that showed increased abundance in the FMT-EF recipient group were also elevated in the donor estropausal females (*Bacteria;Firmicutes;Clostridia;Clostridiales;Ruminococcaceae* and *Bacteria;Firmicutes;Clostridia; Clostridiales;Lachnospiraceae;Coprococcus 2;uncultured organism ;* Figures 5F and S6E). These results indicate that transplanting microbiota from young or estropausal female mice led to changes in the microbial landscape of the recipient mice. Other studies have also reported the selective enrichment of specific microbial species from donor microbiota in recipient subjects[22,64]. These observations may be attributable to variations in the intestinal microenvironments, which allow the proliferation of certain species.

Subsequently, we used PICRUSt2 to predict functional abundance differences between the FMT-YF and FMT-EF groups (Figure 5G). We identified significant functional groups only with up-regulated functional terms in the FMT-EF group, with no significant down-regulated terms. Notably, there was a significant presence of terms related to the menaquinol biosynthesis pathway, including those involved in 1,4-dihydroxy-6-naphthoate biosynthesis II, 1,4-dihydroxy-6-naphthoate biosynthesis I, and the superpathway of menaquinol-8 biosynthesis II (Figure 5G). Menaquinols, the active hydroquinone forms of vitamin K, also known as menaquinones (MKs), facilitate the carboxylation of vitamin K-dependent proteins, which are crucial for biological processes such as blood clotting, bone health, and heart health[65]. Given the stability of menaquinones and their primary synthesis by gut microbiota, we opted to measure these forms in stool samples (MK6-MK13). Furthermore, by focusing on menaquinones, we aim to evaluate their potential systemic effects post-absorption, as they contribute significantly to the host's vitamin K status. However, no significant differences in MKs concentrations in the stool samples of FMT-YF and FMT-EF animals were observed (Figures S6F-G), although this may be the result of high animal-to-animal variability and/or the high vitamin K content of the standard mouse chow at the USC vivarium dietary (see Discussion).

Causal mediation analyses reveal microbial genera potentially influencing ovarian transcriptome

Lastly, we performed causal mediation analyses to characterize microbial genera that may directly influence the ovarian transcriptome remodeling that we observed between FMT-YF and FMT-EF

mice (Figure 6). From the ASVs exhibiting significant abundance variations between the groups, we identified four ASV IDs (850e0d58c1aa35238538564a8010e0ff, e4f32cdc3407edb8423447421078fdae, 55ebdcf041fb6b8b4632993423011372, and d4840c45eb37593108d020fb6a63f8e2) with a significant mediation effect on ovarian transcriptome changes (Figure 6B). Notably, three of these potential mediators belong to the *Muribaculaceae* family. Further exploration of the *Muribaculaceae* family and specific species within the genera will be crucial for understanding their direct impact on the modulation of the ovarian transcriptome.

Discussion

In this study, we examined the fecal microbial profiles of three distinct groups: (1) young and naturally aged estropausal female mice, (2) mice with chemically-induced premature ovarian failure and their control counterparts, and (3) young and naturally aged male mice. Through our comparative analysis, we identified and differentiated between functional pathways that may be unique to ovarian aging (*i.e.* phospholipases pathway) and those specific to general aging (*i.e*. L-lysine biosynthesis I, pyridoxal 5-phosphate biosynthesis I, and superpathway of pyridoxal 5-phosphate biosynthesis). Furthermore, through fecal microbiota transplantation assays, we discovered that alterations in the gut microbiota can significantly impact the ovarian landscape, affecting both fertility and the health state of the ovaries. We also identified specific microbial genera as potential mediators of the observed effects on ovarian function. Future investigations focusing on these genera and the identification of specific species hold significant promise for crafting novel therapeutic strategies aimed at mitigating or potentially reversing ovarian aging.

Ovarian RNA-seq data of the FMT recipients supports causal influence of the gut microbiota on ovarian function

Our analysis of ovarian RNA-seq data from the FMT recipients (FMT-YF vs. FMT-EF) revealed significant changes in the ovarian transcriptome following alterations in the gut microbiota. While existing research underscores the broad effects of the gut microbiome on host health, evidence detailing its direct effects on the transcriptome of various tissues remains sparse. For instance, earlier research demonstrated that mice raised in a germ-free environment exhibit a markedly distinct liver transcriptome compared to their conventionally raised counterparts[26]. To the best of our understanding, the direct influence of gut microbiota on the ovarian transcriptome has not yet been documented. Our analysis not only uncovered significant variations in the ovarian transcriptome among FMT recipient mice (*i.e.* reduced inflammatory pathway in the FMT-EF group), but we also noted the transmission of phenotypic alterations (*i.e*. improved fertility and ovarian health). Collectively, these results offer substantial evidence of gut microbiota's direct role in influencing ovarian function and health. Furthermore, the microbial genera and functional pathways we identified serve as valuable assets for future research aimed at investigating potential therapeutic strategies.

Unexpected advantageous effects of grafting estropausal female fecal microbiota may be due to compensatory mechanisms

Based on previous research that has shown detrimental effects of gut microbiota from donors with ovarian dysfunction, such as PCOS[25], we initially hypothesized that transplanting fecal microbiota from estropausal mice might induce estropause-like phenotypes in the recipient mice. Contrary to our expectations, however, we observed an ovarian transcriptome in the recipients that resembled that of young ovaries, alongside improvements in ovarian health and fertility following the transplantation of microbiota from estropausal females. The unexpected advantageous effects observed could be attributed to a compensatory mechanism. For instance, FSH, required for follicle maturation and ovulation, is found in elevated levels in post-menopausal women and estropausal mice[2,66,67]. After reproductive senescence, the ovaries no longer produce estrogen or mature eggs, so the pituitary gland compensates by producing more FSH in an attempt to stimulate the now non-responsive ovaries[30]. Similarly, it is conceivable that the gut microbiota in reproductively senescent female mice could be enriched with beneficial microbes and/or metabolites that support ovarian health, perhaps as a compensatory response. Cumulative studies have highlighted the role of gut microbiota in compensatory processes. For instance, one study demonstrated that gut microbiota can influence the levels of peptides that regulate energy balance in the hypothalamus, serving as a mechanism to decrease body fat[68]. Furthermore, an increase in microbes that produce metabolites critical for the nervous system's function—such as serotonin, acetylcholine, histamine, and dopamine—was observed in patients with mild cognitive impairment[69]. Therefore, when young adult female mice received fecal microbiota transplants from estropausal females, it is possible that the enriched gut microbial environment contributed to the manifestation of younger or more reproductively active phenotypes in recipient mice.

Potential involvement of MKs in ovarian health and aging

Although our analysis of functional abundance predicted potential shifts in the biosynthesis pathway of MKs in the FMT mice, we observed no significant differences in the stool concentrations of MKs between the FMT-YF and FMT-EF groups. This lack of observable difference might be attributed to

the vitamin K content of the standard chow used by the USC vivarium during our experiments (LabDiet, PicoLab Rodent Diet 20). Specifically, the high vitamin K dietary content could have saturated the system, thus masking subtle variations in MK production by the gut microbiome. Such nuances are typically more pronounced under conditions of a low vitamin K diet[70]. While there have been limited studies, MKs have demonstrated potential benefits for ovarian health in specific contexts, such as certain ovarian cancers and in patients with PCOS[71,72]. Additionally, some studies have underscored the anti-inflammatory properties of MKs[73]. Given our observations of decreased inflammatory function and enhanced ovarian function in the FMT-EF mice, coupled with the documented benefits of MKs, MKs may be therapeutic candidates for improving ovarian health and function. However, further research into the direct effects of MKs on ovarian function will be necessary.

Sex-differences in aging-associated gut microbial profiles

In our comparative study, while we detected certain similarities in the microbial profiles of both females and males with aging, our analysis primarily revealed notable differences between the sexes. Specifically, while aging was associated with significant changes in alpha diversity in female mice, such changes were not observed in males. Moreover, our analyses of differential abundance of microbial genera and predictions of functional abundance revealed substantial differences in the gut microbial profiles and their functions between females and males as they age. Indeed, extensive research has established that aging manifests differently in females and males, a phenomenon known as sex dimorphism in aging[74]. Particularly, the susceptibility to diseases associated with aging, including Alzheimer's disease and obesity, varies significantly between the sexes[75-77]. Furthermore, the disparity in lifespan between females and males is consistently observed across various species[78,79]. In agreement with our findings in this study, sex differences in the gut microbiome associated with aging have previously been documented[80,81]. While the limited number of existing studies suggest a possible influence of sex hormones on the observed sex differences in the gut microbial profiles[82-84], these findings do not negate the potential effects of non-hormonal factors, such as those related to sex chromosomes, on the differences noted between sexes. Given the significant distinctions between sexes highlighted in this study and their varied impacts, it is imperative to consider sex as a contributing factor in future gut

microbiome research, not only to deepen our understanding but also to address the specific differences effectively.

In summary, we performed a comparative analysis of microbial profiles among aging female, aging male and a chemically-induced menopause model mice to characterize microbial genera that are unique to general aging vs. ovarian aging. Our work highlights potential microbial genera and functional pathways that may play key roles in modulating ovarian function.

Limitations of the study

Our study's findings are limited by the use of 16S rRNA amplicon sequencing for gut microbiome analysis. While this method is valuable for identifying broader microbial community structures, it lacks the resolution to pinpoint specific species driving the observed effects on ovarian health and the transcriptome. To investigate these intricate microbial-host interactions, transitioning to full metagenomic sequencing will be important in future studies. This technique will allow for the identification of individual microbial species and their genomic functions, offering a deeper insight into their roles in host health. Additionally, experimenting with FMT from young and estropausal females to those of middle-aged (7-9-months) could further illuminate the microbiome's impact on ovarian function at a crucial transitional period before mice become estropausal. Future studies employing full metagenomic sequencing and exploring FMT from different female reproductive stages will significantly enhance our understanding of the intricate impact the microbiome on female reproductive health throughout different life phases.

Acknowledgements

We thank Dr. Victor Ansere and Dr. Juan Bravo for feedback on our manuscript. This work was supported by the GCRLE-2020 post-doctoral fellowship from the Global Consortium for Reproductive Longevity and Equality at the Buck Institute, made possible by the Bia-Echo Foundation to M.K., USC Provost's Undergraduate Research Fellowship to J.W., National Institute on Aging (NIA) T32 AG052374 predoctoral fellowship and Diana Jacobs Kalman/AFAR Scholarships for Research in the Biology of Aging to R.J.L., and Pew Biomedical Scholar award #00034120 from the Pew Charitable Trust to B.A.B. Ovarian histological analysis was performed by the Translational Pathology Core at the USC Norris Comprehensive Cancer Center (supported by NCI P30 CA014089). Serum hormone quantification was performed by the University of Virginia Center for Research in Reproduction Ligand Assay and Analysis Core (supported by the Eunice Kennedy Shriver NICHD/NIH Grant R24HD102061). Stool vitamin K concentrations were supported by the USDA Agricultural Research Service under Cooperative Agreement No. 58-1950-7-707. Any opinions, findings, conclusions, or recommendations expressed in this publication are those of the authors and do not necessarily reflect the views of the USDA.

Author contributions

M.K. and B.A.B. designed the study. M.K. performed live animal experiments. M.K. and R.L.J. dissected mouse tissues. M.K., J.W. and Y.K analyzed ovarian histology data. M.L., X.F. and S.L.B quantified stool MK concentrations. M.K. and J.W. performed computational analyses. M.K. and B.A.B. wrote the manuscript with input from all authors. All authors edited and commented on the manuscript.

Declaration of interests

The authors declare no competing interests.

Figure legends

Figure 1. Characterization of ovarian health state and fecal microbial profiles of young and estropausal female mice. (A) Schematic diagram of the experimental setup of female aging cohorts. (B) Box plot of ovarian health index of young and estropausal mice. (C) Principal component analysis result of CLR-transformed and batch-corrected ASV counts from young and estropausal female mice. Animals from four independent cohorts (C1-C4), n=19-20 per group (variation due to animal death prior to experiment; n=20 for young females; n=19 for estropausal females). (D) Box plots of Observed features, Evenness Pielou, Shannon entropy and Faith PD indices of young and estropausal female mice. Medians from young females for each cohort were used to normalize indices. (E) Differential abundance analysis results of microbial genera of young vs. estropausal female mice using ALDEx2. (F) Functional abundance prediction analysis of young vs. estropausal female mice using PICRUSt2. Significance in nonparametric two-sided Wilcoxon rank-sum tests are reported for (B) and (D). YF: Young female; EF: Estropausal female. C: Cohort.

Figure 2. Bulk RNA-seq analysis of ovaries from young and estropausal female mice fecal microbiota transplantation recipient mice. (A) Schematic diagram of the experimental setup of fecal microbiota transplantation (FMT) cohort. (B) Multidimensional scaling (MDS) analysis result of RNA expression between young and estropausal female mice FMT recipient mice (FMT-YF and FMT-EF, respectively). (C) Heat map of significant (FDR < 5%) genes differentially expressed in FMT-YF vs. FMT-EF mice. (D-G) Top GSEA enriched terms from (D) Gene Ontology Biological Process (GO BP), (E) Gene Ontology Molecular Function (GO MF), (F) Gene Ontology Cellular Component (GO CC) and (G) Gene Transcription Regulation Database (GTRD – TF targets). Only up to top ten most-upregulated and top ten most-downregulated gene sets are plotted for readability.

Figure 3. Analysis of public ovarian aging bulk RNA-seq datasets. (A) Schematic diagram of the analysis setup of public ovarian aging bulk RNA-seq datasets, CRA003645 and PRJNA1002222, from young (2-3-months) and estropausal (12-months) female mice. (B-C) GSEA enrichment score plots of (B)

genes that are up-regulated with ovarian aging ("UP with ovarian aging", left panel) and down-regulated with ovarian aging ("DOWN with ovarian aging, right panel), and (C) SenMayo gene set. DGE: Differential gene expression.

Figure 4. Evaluation of fertility and ovarian health state of fecal microbiota transplantation recipient mice. (A) Schematic diagram of the experimental setup. (B) Box plot of ovarian health index of FMT-YF and FMT-EF mice. (C) Box plot of pup counts of first litters of young and estropausal female mice fecal microbiota transplantation recipient mice (FMT-YF and FMT-EF, respectively). Pup counts were measured from two independent cohorts (n=8 per group and n=16 per cohort). (D) Reproductive success rate analysis result shown as percentages of nulliparous between FMT-YF and FMT-EF. Significance in nonparametric two-sided Wilcoxon rank-sum tests are reported for (B) and (C), and logrank test for (D).

Figure 5. Characterization of fecal microbial profiles of fecal microbiota transplantation recipient mice. (A) Schematic diagram of the experimental setup. (B) Principal component analysis result of CLR-transformed and batch-corrected ASV counts from young and estropausal female mice fecal microbiota transplantation recipient mice (FMT-YF and FMT-EF, respectively). (C) Principal coordinate analysis results of Bray-Curtis dissimilarity (left panel) and Jaccard (right panel) indices. (D) Box plots of Observed features, Evenness Pielou, Shannon entropy and Faith PD indices of FMT-YF and FMT-EF mice. (E) Differential abundance analysis results of microbial genera of FMT-YF vs. FMT-EF mice using ALDEx2. (F) Venn diagram of overlapping microbial genera between genera that increase in abundance with female aging ("UP in EF") and increase in abundance in FMT-EF recipient mice ("UP in FMT-EF"). (G) Functional abundance prediction analysis of FMT-YF vs. FMT-EF mice using PICRUSt2. Significance in nonparametric two-sided Wilcoxon rank-sum tests are reported for (D). YF: Young female; EF: Estropausal female.

Figure 6. Causal mediation analysis of amplicon sequence variants and ovarian transcriptome changes in fecal microbiota transplantation recipient mice. (A) Graphical representation of causal

mediation analysis. (B) Causal mediation analysis results of amplicon sequence variants (ASVs) that showed significant mediation effects on changes in the ovarian transcriptome in fecal microbiota transplantation recipient mice. Nonparametric bootstrap confidence intervals with the percentile method are reported. ACME: Average Causal Mediated Effect; ADE: Average Direct Effect.

STAR Methods

Key resources table

REAGENT or RESOURCE	SOURCE	IDENTIFIER
Chemicals, peptides, and recombinant proteins		
Bouin's solution	Sigma	HT10132
Ampicillin	Sandoz	00781
Amphotericin-B	Sigma	A9528
Metronidazole	MFR VIONA PHARMACEUTICALS	096988
Vancomycin	Alvogen	Vet-Rx-MW 090160
Neomycin	MFR VETONE	510570
Trizol	Ambion	15596018
Critical commercial assays		
The Rat and Mouse Anti-Müllerian hormone (AMH) enzyme-linked immunosorbent assay (ELISA) kit	Ansh Labs	AL-113
Millipore Pituitary Panel Multiplex kit	Millipore	RPT86K
Inhibin A (The animal Inhibin A enzyme linked immunosorbent assay (ELISA) kit	Ansh Labs	AL-161
QIAamp Fast DNA Stool Mini Kit	QIAGEN	51604
Direct-zol RNA Miniprep	Zymo Research	R2052
Deposited data		
FASTQ reads of 16S rRNA V3-V4 amplicon sequencing dataset – Young vs. estropausal females, Young vs. old males, control vs. VCD-injected female mice and FMT-YF vs. FMT-EF recipient mice	This study	PRJNA1076509

FASTQ reads of bulk mRNAseq of FMT-YF and FMT-EF ovaries	This study	PRJNA1076509
Microscopy images of ovarian hematoxylin and eosin staining slides	This study	Figshare DOIs: 10.6084/m9.figshare.25749588, 10.6084/m9.figshare.25749594, 10.6084/m9.figshare.25749591
Bulk RNA-seq dataset of wild-type young (3-months) vs. aged/estropausal (12-months) ovaries from mice	Zhou, Z., et al.[65]	CRA003645
Bulk RNA-seq dataset of wild-type young (2-months) vs. aged/estropausal (12-months) ovaries from mice	Yang, Q., et al.[66]	PRJNA1002222
Experimental models: Organisms/strains		
C57BL/6JNia	NIA Aging colony at Charles River Laboratories	C57BL/6JNia – Female, 3- and 19-months
C57BL/6JNia	NIA Aging colony at Charles River Laboratories	C57BL/6JNia – Male, 3- and 19-months
C57BL/6NTac – 3.5-month-olds	Taconic Biosciences	B6-F
C57BL/6NTac – 3.5-month-olds	Taconic Biosciences	B6-M
Software and algorithms		
Code for this study	This study	https://github.com/BenayounLaboratory/Ovarian_Aging_Microbiome

bapred v. 1.1	Hornung, R., et al.[85]	https://cran.r-project.org/web/packages/bapred/index.html
CSCDRNA v. 1.0.3	Jew, B., et al.[86]	https://github.com/empiricalbayes/CSCDRNA
DescTools v. 0.99.50	Signorell, A.[87]	https://cran.r-project.org/web/packages/DescTools/index.html
DESeq2 v. 1.34.0	Love, M.I., et al.[88]	https://bioconductor.org/packages/release/bioc/html/DESeq2.html
Fastx Trimmer v. 0.0.14	Gordon, A.[89]	http://hannonlab.cshl.edu/fastx_toolkit/
Granulator v. 1.2.0	Newman, A.M., et al.[90]	https://github.com/Novartis/granulator
HOMER v. 4.11.1	Heinz, S., et al.[91]	http://homer.ucsd.edu/homer/ngs/
limma v. 3.50.1	Ritchie, M.E., et al.[92]	https://bioconductor.org/packages/release/bioc/html/limma.html
mediation v. 4.5.0	Tingley, D., et al.[93]	https://cran.r-project.org/web/packages/mediation/

mixOmics v. 6.18.1	Rohart, F., et al.[94]	https://bioconductor.org/packages/release/bioc/html/mixOmics.html
QIIME2 v. 2023.7	Bolyen, E., et al.[95]	https://qiime2.org/
qiime2R v. 0.99.6	Bisanz, J.[96]	https://github.com/jbisanz/qiime2R
STAR v. 2.7.9a	Dobin, A., et al.[97]	https://hbctraining.github.io/Intro-to-rnaseq-hpc-O2/lessons/03_alignment.html
sva v. 3.42.0	Leek, J. T. and Sotrey, J.D.[98]	https://bioconductor.org/packages/release/bioc/html/sva.html
subread v. 2.0.3	Liao, Y., Smyth, G.K., and Shi, W.[99]	https://subread.sourceforge.net/
Trim Galore v. 0.6.6	Krueger, F.[100]	https://www.bioinformatics.babraham.ac.uk/projects/trim_galore/
Other		
MiniCollect® Serum Tube	Greiner	450472
Lysing Matrix D tubes	MP	6913500
BeadBug 6 microtube homogenizer	Benchmark Scientific	D1036
4200 TapeStation system	Agilent	G2991A
High Sensitivity RNA ScreenTapes	Agilent	5067–5579

Keyence BZ-X710	Keyence	BZ-X

Resource availability

Lead contact

Further information and requests for resources and reagents should be directed to and will be fulfilled by the lead contact, Bérénice A. Benayoun (berenice.benayoun@usc.edu).

Materials availability

No new materials were generated for this study.

Data and code availability

The raw FASTQ files have been deposited to the Sequence Read Archive under accession PRJNA1076509. Raw microscopy pictures of ovarian hematoxylin and eosin staining are available on Figshare (Figshare DOIs: 10.6084/m9.figshare.25749588, 10.6084/m9.figshare.25749594, 10.6084/m9.figshare.25749591). All scripts used to analyze this dataset are available on the Benayoun lab GitHub at https://github.com/BenayounLaboratory/Ovarian_Aging_Microbiome. All R code was run using R 4.1.2. Any additional information required to reanalyze the data reported in this work paper is available from the lead contact upon request.

Experimental model and study participant details

Mouse husbandry

All animals were treated and housed in accordance with the Guide for Care and Use of Laboratory Animals. All experimental procedures were approved by the USC's Institutional Animal Care and Use Committee (IACUC) and are in accordance with institutional and national guidelines. Samples were derived from animals on approved IACUC protocol number 20770 and 21212.

For the "aging cohort," female and male C57BL/6JNia mice (4- and 20-month-old animals) were obtained from the National Institute on Aging (NIA) colony at Charles River Laboratories. For the "VCD

cohort" and "fecal microbiota transplantation (FMT) cohort", female C57BL/6NTac mice (3.5-month-old animals) were ordered from Taconic Biosciences. All animals were acclimated at the specific-pathogen-free animal facility at USC for 2 weeks before any processing. All animals were fed PicoLab Rodent Diet 20 (LabDiet, 5053). The facility is on a 12-h light/dark cycle and animal housing rooms are maintained at 72 °F and 30 % humidity. All animals were euthanized between 8–11 am, by CO_2 asphyxiation followed by cervical dislocation.

Method details

Ovarian follicle counts

Ovaries were fixed in Bouin's solution (Sigma, HT10132) for 24 hrs at room temperature and transferred to 70 % ethanol for storage. Paraffin embedding, tissue sectioning and staining with hematoxylin and eosin (H&E) were performed by the USC Norris Comprehensive Cancer Center Translational Pathology Core Facility. H&E staining slides were imaged on the Keyence BZ-X All-in-One Fluorescence Microscope platform. Three sections per ovary were used to count the number of primordial, primary, secondary, and antral follicles and corpus luteum by three blinded observers. Median counts across the 3 observers were used for data analysis. Statistical significance between groups was assessed using the non-parametric Wilcoxon rank-sum test.

Quantification of serum AMH, FSH and Inhibin A concentrations

After euthanasia, blood was collected directly from the heart. Blood was allowed to clot at room temperature for 1 hour, and serum was separated using MiniCollect® Serum Tube (Greiner, 450472), then stored at -80 °C until further processing. Quantification of serum AMH (Rat and Mouse Anti-Müllerian hormone (AMH) ELISA kit, Ansh Labs, AL-113), FSH (Millipore Pituitary Panel Multiplex kit, RPT86K), and Inhibin A (Inhibin A ELISA kit, Ansh Labs, AL-161) levels were performed by the University of Virginia Center for Research in Reproduction Ligand Assay and Analysis Core. Standard normalized values were provided by the core. Statistical significance between groups was assessed using the non-parametric Wilcoxon rank-sum test.

Ovarian health index calculation

The ovarian health index was calculated by analyzing levels of ovarian hormones (AMH, FSH, and Inhibin A) and follicle counts (combined counts of primordial, primary, secondary, and antral follicles and corpus luteum), using their quartile distributions. We designed the scoring system to reflect the biological significance of these markers – favoring higher AMH levels and follicle counts, and lower FSH and Inhibin A levels. We then segmented the data into quartiles, assigning each a score from 1 to 4 based on their health implications. The index was derived by averaging the scores for each indicator (ovarian hormone level and follicle count scores) per individual. To enhance interpretability, the score was scaled to a 0-100 percentile format. Statistical significance between groups was assessed using the Wilcoxon rank-sum test.

Scripts used to calculate the ovarian health index are available on the Benayoun lab GitHub at https://github.com/BenayounLaboratory/Ovarian_Aging_Microbiome.

DNA extraction for 16S rRNA amplicon analysis

Fecal matter for 16S rRNA V3-V4 amplicon analysis were collected aseptically post-euthanasia. Samples were immediately snap frozen in sterile tubes and stored at -80 °C. DNA extraction was performed using QIAamp Fast DNA Stool Mini Kit (QIAGEN, 51604), following the manufacturer's protocol.

V3-V4 region targeted amplification and sequencing were performed by Novogene Inc. Amplification primers used were CCTAYGGGRBGCASCAG (FWD_341F) and GGACTACNVGGGTWTCTAAT (REV_806R). Amplicon libraries were sequenced on the Illumina NovaSeq 6000 machine. De-multiplexed FASTQ files were provided by Novogene Inc. for data analysis.

16S rRNA V3-V4 amplicon sequencing data analysis

<u>Data pre-processing, quality control and denoising</u>

Data pre-processing, quality control and denoising were performed within the QIIME2[95] (v. 2023.7) platform. Each cohort was analyzed independently for memory and computing efficiency. FASTQ files were imported to QIIME2 and denoised using DADA2[101]. Forward and reverse reads were truncated at

226 bp and 224 bp, respectively, to obtain reads with quality scores above 25 and to ensure coverage of the V3-V4 region (–p-trunc-len-f 226 –p-trunc-len-r 224).

Batch correction and principal component analysis of amplicon sequence variants

Previous studies have shown that effectiveness of batch correction tools are dataset-dependent[102]. For batch correction, a previously described benchmarking pipeline[102] was used to select the most effective batch correction tool for our dataset. removeBatchEffect function from limma[92] (v. 3.50.1), Combat from sva[98] (v. 3.42.0) and FAbatch from bapred[85] (v. 1.1) were benchmarked. Denoised feature tables were imported to R using qiime2R[96] package (v. 0.99.6). Then, features with low counts (less than 0.01% of all the counts) were removed and filtered counts were centered log ratio (CLR)-transformed. Based on principal component analysis results (method described below) and variance calculations, FAbatch-corrected values were chosen for downstream analyses.

Principal component analysis of amplicon sequence variants

For principal component analysis (PCA), pca function from mixOmics[94] (v. 6.18.1) was used in R. For female and male aging cohorts, FAbatch-corrected values were used for PCA. For VCD and FMT cohorts, CLR-transformed values were used for PCA.

Beta diversity and alpha diversity analyses

For beta and alpha diversity analyses, phylogenetic trees were generated using the ‘qiime phylogeny align-to-tree-mafft-fasttree’ command. Rooted phylogenetic trees were used to run the ‘qiime diversity core-metrics-phylogenetic’ command for beta and alpha diversity analyses. Diversity analysis results were imported to R using qiime2R[96] package (v. 0.99.6) for further plot generation and significance tests. Bray-Curtis dissimilarity and Jaccard index principal coordinate analysis results were used to generate beta diversity plots using ggplot2 (v. 3.4.2). Alpha diversity box plots were generated based on observed features, evenness Pielou, Shannon entropy and Faith’s phylogenetic diversity (PD) indices. Median values of each sex or group (*i.e*. CTL vs. VCD and FMT-YF vs. FMT-EF) within each cohort were used for normalization in combined. Additionally, separate plots displaying raw index values for each

cohort were generated. The statistical significance of differences in alpha diversity between groups was determined using the Wilcoxon rank-sum test.

Differential abundance analysis of microbial genera

Differential abundance analysis of microbial genera was performed using the ALDEx2[103] plugin within the QIIME2[95] platform. Taxonomic classifier was generated using the SILVA[104] (132 release) reference. Reference reads were extracted for CCTAYGGGRBGCASCAG (FWD_341F) and GGACTACNVGGGTWTCTAAT (REV_806R) primer set and a classifier was trained using the 'qiime feature-classifier extract-reads' and 'qiime feature-classifier fit-classifier-naive-bayes' commands, respectively. Differential abundance analysis results and taxonomic classifier were imported to R using qiime2R[96] for comparative analysis and plot generation. For female and male aging cohorts, differential abundance analysis results for each cohort for each sex was combined based on the directionality of the differential abundance measures, identifying features that consistently exhibited either an increase or decrease across all cohorts for each sex. Using Fisher's method and Benjamini-Hochberg (BH) correction method, p-values for each feature's differential abundance were combined and corrected, respectively. Additionally, the mean of effect size across cohorts for each feature was used for analysis. For combined female and aging cohorts, as well as VCD and FMT cohorts, features with an adjusted p-value < 0.05 and an absolute effect size > 1 were identified as significantly different in abundance.

Functional abundance prediction analysis

Functional abundance prediction analysis was performed via the PICRUSt2[42] plugin within the QIIME2[95] platform using default parameters. PICRUSt2 results were imported to R using qiime2R. For differential abundance and statistical significance analyses, ALDEx2[103] was used (500 Monte Carlo samples, Wilcoxon test for statistical testing, effect size calculation enabled, and the interquartile log ratio (iqlr) for denominator calculation). To combine independent cohorts for female and male aging cohorts, Fisher's method and Benjamini-Hochberg multiple testing correction were used to combine and correct the p-values. Also, the mean values of effect sizes were calculated for each feature. Adjusted p-value less

than 0.05 and absolute effect size greater than 1 were used as criteria to filter functional pathways that were significantly different in abundance.

Fecal microbiota transplantation

For fecal microbiota transplantation (FMT), animals underwent a 10-day course of antibiotics/antimycotic (Ab/Am) treatment before transplantation. The regimen included ampicillin in drinking water at 1 g/L (Sandoz, 00781), and oral gavage of amphotericin-B (Sigma, A9528) at 1 mg/kg/day, metronidazole (MFR VIONA PHARMACEUTICALS, 096988) at 100 mg/kg/day, vancomycin (Alvogen, Vet-Rx-MW 090160) at 50 mg/kg/day, and neomycin (MFR VETONE, 510570) at 100 mg/kg/day. Starting on the third day after the end of the Ab/Am treatment, FMT was performed biweekly for three weeks via oral gavage. Donor stool samples from young or estropausal female mice were prepared by suspending in saline (20 mg/ml), followed by vortexing and centrifugation to obtain the supernatant. Each recipient animal received 100 µl of the fecal suspension. Sample collection for subsequent processing and analysis occurred three days after the final FMT session.

Ovarian RNA-seq sample preparation

Ovaries were harvested and immediately snap-frozen in sterile tubes, and then stored at -80 °C. For RNA extraction, 600 µl of Trizol reagent (Ambion, 15596018) was added to the ovaries in Lysing Matrix D tubes (MP, 6913500) and tissues were homogenized with a BeadBug 6 microtube homogenizer (Benchmark Scientific, D1036) at 3,500 rpm for 30 seconds for 3 cycles in the cold room. Total RNA was purified using the Direct-Zol RNA Miniprep (Zymo Research, R2052), following the manufacturer's instructions. Integrity and quality of the purified total RNA were assessed on the 4200 TapeStation system (Agilent, G2991A) using High Sensitivity RNA ScreenTapes (Agilent, 5067–5579) to determine the RNA Integrity Number (RIN). Subsequently, mRNA-seq libraries were prepared and sequenced by Novogene Inc. to obtain PE150 sequencing reads on the NovaSeq X Plus platform.

FMT cohort ovarian RNA-seq data analysis

<u>Data quality control and pre-processing</u>

Paired-end 150-bp reads were hard-trimmed to remove the first 6 bases and keep up to 100bp using Fastx Trimmer[89] (v. 0.0.14) and processed using Trim Galore[100] using default parameters (v. 0.6.6). Trimmed reads were mapped to the mm39 genome reference using STAR[97] (v. 2.7.9a). Read counts were assigned to genes from the mm39 genome reference using subread[99] (v. 2.0.3). After assigning read counts to genes, downstream processing was performed in R (v. 4.1.2). Low count genes (genes with less than 1 count in at least 6 out of 14 RNA-seq libraries) were removed to improve memory and speed efficiency of DESeq2[88], as recommended by the developers. We used surrogate variable analysis to estimate and correct for unwanted experimental noise. R package sva[98] (v. 3.42.0) was used to estimate surrogate variables and the removeBatchEffect function from limma[92] (v. 3.50.1) was used to regress out the effects of surrogate variables and RNA integrity differences (RNA integrity number scores) from raw read counts. To remove extreme values within the read counts, Winsorize function from DescTools[87] (v. 0.99.50) was used to adjust the values above the 99.9th percentile to the values at the 99.9th percentile. DESeq2[88] package (v. 1.34.0) was used for downstream analyses of the RNA-seq data. Genes with FDR < 5% were considered statistically significant. For the multidimensional scaling (MDS) analysis, we calculated the distance between samples using the inverse of Spearman's rank correlation coefficient (1-Rho) as the distance metric. These distances were then input into the cmdscale function in R to compute the MDS coordinates.

<u>Gene ontology analysis of RNA-seq dataset</u>

We used the GSEA[49] approach through the phenoTest package. GO term annotations were sourced from the Molecular Signature Database[105] (ENS.GO.BP, ENS.GO.MF, ENS.GO.CC and GTRD gene sets). The t-statistic from DESeq2[88] was used to rank genes for functional enrichment analysis. For readability, only the top ten most-significant pathways with negative NES and top ten most-significant pathways with positive NES are shown in figures if more than that passed the FDR < 5% significance threshold for GO terms and FDR < 10% for GTRD transcription factor targets (see main text for explanation).

<u>Deconvolution analysis of immune cell type proportion</u>

To estimate any differences in the immune cell proportions between FMT-YF and FMT-EF groups of the FMT cohort, single-cell RNA-seq reference-based deconvolution analyses were performed, using CSCDRNA[86] and Granulator[90]. We downloaded the cell type annotated Seurat object of a publicly available murine ovarian single-cell RNA-seq dataset (Open Science Framework dataset ID 924fz)[50]. In the CSCDRNA analysis, the min.p parameter was set to 0.3 following the authors' recommendation[86], to efficiently exclude the 30% least significant portion of marker genes for each cell type. This threshold was chosen to increase efficiency and reduce noise. For Granulator, the qprogwc method[106] was used with default parameters to estimate the immune cell proportions within the ovarian bulk RNA-seq dataset. Cell proportions were tested for significance using a Wilcoxon test rank-sum test.

Pre-processing and filtering candidate transcription factor-bound genes

For potential transcription factors identified from GSEA[49] analysis against GTRD[53] transcription factor targets, peak information was obtained for Cistrome.org. Peak annotation was performed using HOMER[91]. Genes with peaks annotated in TSS-promoter of protein coding genes were considered direct target genes. Obtained gene lists were used to perform GSEA through the phenoTest package.

Pre-processing of public ovarian aging datasets

To evaluate the correlation between ovarian aging and FMT gene expression profiles of the ovaries, we pre-processed and analyzed two publicly available ovarian aging datasets (2-3-month-old vs. 12-month-old female mice; BioProject dataset PRJNA100222 and GSA dataset CRA003645)[60,61]. For each dataset, reads were pre-processed and aligned to the mm39 genome reference using the same methods as for the FMT cohort ovarian RNA-seq dataset. Low count genes (genes with less than 1 count in at least 4 out of 7 RNA-seq libraries) were removed. sva[98] (v. 3.42.0) was used to estimate surrogate variables and the removeBatchEffect function from limma[92] (v. 3.50.1) was used to regress out the effects of surrogate variables from raw read counts. DESeq2[88] package (v. 1.34.0) was used for downstream analyses of the RNA-seq data. p-values for common genes between the two datasets were combined and corrected using Fisher's method and BH correction method, respectively. FDR < 0.001% was used to

catalog gene sets that are robustly up- or down-regulated with aging. Obtained gene lists were used to perform GSEA through the phenoTest package.

Fertility assay

Fertility assay was performed as previously described[63]. FMT female mice were paired with 4-month-old males at a 1:1 ratio 3 days after the last day of FMT administration until the birth of the first litter. The number of pups in the first litter and the latency, defined as the duration between the pairing date and the birth date of the first litter, were recorded and analyzed. Statistical difference in latency in the 1st litter after pairing was evaluated using a log-rank test.

Stool menaquinone concentration quantification

Frozen stool samples were shipped to the Vitamin K Laboratory at the Tufts University Human Nutrition Research Center on Aging (HNRCA), where stool menaquinone-5 through 13 concentrations were measured using the LC/MS and menaquinone-4 and phylloquinone concentrations were measured by HPLC, as detailed elsewhere[107]. The lowest limit of detection for stool menaquinones ranges from 10 (menaquinone-6) to 0.1 (menaquinone-4 and phylloquinone) pmol/g[107].

Causal mediation analysis

Causal mediation analysis to identify specific amplicon sequence variants (ASVs) from the FMT cohort acting as mediators between the treatment (FMT-YF vs. FMT-EF) and outcome (changes in the ovarian transcriptome profiles) was performed using mediation package[93] (v. 4.5.0) in R. Feature table, taxonomic reference and differential abundance analysis results generated from QIIME2[95] were imported to R using qiime2R[96]. ASVs identified as significant in differential abundance analyses were tested. CLR-transformed ASV counts were used for the mediation analyses. For the outcome variable, the first dimension from the multidimensional scaling (MDS) analysis of the FMT ovarian mRNAseq dataset was used. Linear models were constructed for both the mediator and the outcome, incorporating the treatment as an independent variable in each. The mediate function from the mediation package was then

employed to estimate the Average Causal Mediation Effects (ACME), Average Direct Effects (ADE), and Total Effects.

Quantification and statistical analysis

All statistical analysis was performed using the R software, version 4.2.4. For all boxplots, the data is shown with the median, the 25th and 75th percentile of the data, and the whiskers represent 1.5 $*$ the inter-quartile range (IQR). Individual datapoints are always overlayed for transparency and rigor. Specific statistical tests used, the number of biological replicates and how many animals they are indicated in the corresponding figure legends and associated method section.

Supplementary information – Supplementary figure legend

Supplementary Figure 1. Characterization of ovarian health state and fecal microbial profiles of young and estropausal female mice. (A) Representative images of ovarian hematoxylin-eosin stained sections. Scale bar: 50 µm. (B) Box plots of ovarian follicle counts per section. (C) Stacked bar plot of cumulative ovarian follicle counts per section from five animals per group. (D) Box plots of serum concentrations of AMH, FSH and Inhibin A. (E) Principal coordinate analysis results of Bray-Curtis dissimilarity (top panel) and Jaccard (bottom panel) indices. Significance in nonparametric two-sided Wilcoxon rank-sum tests are reported for (B) and (D). YF: Young female; EF: Estropausal female.

Supplementary Figure 2. Characterization of ovarian health state of VCD cohort mice. (A) Schematic diagram of the experimental setup of VCD cohort. (B) Box plot of ovarian health index of control and VCD-injected mice. (C) Representative images of ovarian hematoxylin-eosin stained sections. Scale bar: 50 µm. (D) Box plots of ovarian follicle counts per section. (E) Stacked bar plot of cumulative ovarian follicle counts per section from five animals per group. (F) Box plots of serum concentrations of AMH, FSH and Inhibin A. Significance in nonparametric two-sided Wilcoxon rank-sum tests are reported for (B), (D) and (F).

Supplementary Figure 3. Characterization of fecal microbial profiles of VCD cohort mice. (A) Principal component analysis result of CLR-transformed and batch-corrected ASV counts from control and VCD-injected mice. (B) Principal coordinate analysis results of Bray-Curtis dissimilarity (top panel) and Jaccard (bottom panel) indices. (C) Box plots of normalized Observed features, Evenness Pielou, Shannon entropy and Faith PD indices. Median from control-injected mice was used to normalize indices. (D) Differential abundance analysis results of microbial genera of control vs. VCD-injected mice using ALDEx2. (E) Functional abundance prediction analysis of control vs. VCD-injected mice using PICRUSt2. Significance in nonparametric two-sided Wilcoxon rank-sum tests are reported for (C).

Supplementary Figure 4. Characterization of fecal microbial profiles of young and old male mice.

(A) Schematic diagram of the experimental setup of male aging cohorts. (B) Principal component analysis result of CLR-transformed and batch-corrected ASV counts from young and old male mice. Animals from three independent cohorts, n=14 per group (variation due to animal death or abnormal health issues prior to experiment). (C) Principal coordinate analysis results of Bray-Curtis dissimilariy (top panel) and Jaccard (bottom panel) indices. (D) Box plots of Observed features, Evenness Pielou, Shannon entropy and Faith PD indices of young and old male mice. Medians from young males for each cohort were used to normalize indices. (E) Differential abundance analysis results of microbial genera of young and old male mice using ALDEx2. (F) Functional abundance prediction analysis of young vs. old male mice using PICRUSt2. Significance in nonparametric two-sided Wilcoxon rank-sum tests are reported for (D). YM: Young male; OM: Old male.

Supplementary Figure 5. Bulk RNA-seq analysis of ovaries from young and estropausal female mice fecal microbiota transplantation recipient mice. (A) Dot plots of immune cell proportions in percentages between young and estropausal fecal microbiota transplantation recipient mice (FMT-YF and FMT-EF, respectively) predicted by deconvolution analyses using CSCDRNA (left panel) and Granulator (right panel). (B) GSEA enrichment score plots Ncoa1-peak (left panel) and Usp7-peak (right panel) genes. (C) Bar plots of normalized $\log_2$ counts of *Ncoa1* and *Usp7* expression.

Supplementary Figure 6. Characterization of ovarian health state and fecal microbial profiles of FMT cohort mice. (A) Representative images of ovarian hematoxylin-eosin stained sections. Scale bar: 50 µm. (B) Box plots of ovarian follicle counts per section. (C) Stacked bar plot of cumulative ovarian follicle counts per section from seven animals per group. (D) Box plots of serum concentrations of AMH, FSH and Inhibin A. (E) Bar plots of CLR-transformed counts of *Ruminococcaceae* and *Lachnospiraceae* from FMT-YF and FMT-EF. (F) Stool concentrations of combined vitamin K (MK6-MK13) of FMT-YF and FMT-EF. (G) Fold change in stool concentrations of vitamin K (MK6-MK13) of FMT-YF and FMT-EF. Significance in nonparametric two-sided Wilcoxon rank-sum tests are reported for (B) and (D).

References

1. Davis, S.R., Lambrinoudaki, I., Lumsden, M., Mishra, G.D., Pal, L., Rees, M., Santoro, N., and Simoncini, T. (2015). Menopause. Nat Rev Dis Primers *1*, 15004. 10.1038/nrdp.2015.4.
2. Broekmans, F.J., Soules, M.R., and Fauser, B.C. (2009). Ovarian aging: mechanisms and clinical consequences. Endocr Rev *30*, 465-493. 10.1210/er.2009-0006.
3. Faddy, M.J., and Gosden, R.G. (1996). A model conforming the decline in follicle numbers to the age of menopause in women. Hum Reprod *11*, 1484-1486. 10.1093/oxfordjournals.humrep.a019422.
4. Fu, C., Hao, W., Shrestha, N., Virani, S.S., Mishra, S.R., and Zhu, D. (2022). Association of reproductive factors with dementia: A systematic review and dose-response meta-analyses of observational studies. EClinicalMedicine *43*, 101236. 10.1016/j.eclinm.2021.101236.
5. Shuster, L.T., Rhodes, D.J., Gostout, B.S., Grossardt, B.R., and Rocca, W.A. (2010). Premature menopause or early menopause: long-term health consequences. Maturitas *65*, 161-166. 10.1016/j.maturitas.2009.08.003.
6. Muka, T., Oliver-Williams, C., Kunutsor, S., Laven, J.S., Fauser, B.C., Chowdhury, R., Kavousi, M., and Franco, O.H. (2016). Association of Age at Onset of Menopause and Time Since Onset of Menopause With Cardiovascular Outcomes, Intermediate Vascular Traits, and All-Cause Mortality: A Systematic Review and Meta-analysis. JAMA Cardiol *1*, 767-776. 10.1001/jamacardio.2016.2415.

850 7. Ossewaarde, M.E., Bots, M.L., Verbeek, A.L., Peeters, P.H., van der Graaf, Y., Grobbee,
851 D.E., and van der Schouw, Y.T. (2005). Age at menopause, cause-specific mortality and
852 total life expectancy. Epidemiology *16*, 556-562. 10.1097/01.ede.0000165392.35273.d4.
853 8. Hong, J.S., Yi, S.W., Kang, H.C., Jee, S.H., Kang, H.G., Bayasgalan, G., and Ohrr, H. (2007).
854 Age at menopause and cause-specific mortality in South Korean women: Kangwha
855 Cohort Study. Maturitas *56*, 411-419. 10.1016/j.maturitas.2006.11.004.
856 9. Knobil, E. (1980). The neuroendocrine control of the menstrual cycle. Recent Prog Horm
857 Res *36*, 53-88. 10.1016/b978-0-12-571136-4.50008-5.
858 10. Santoro, N., Roeca, C., Peters, B.A., and Neal-Perry, G. (2021). The Menopause Transition:
859 Signs, Symptoms, and Management Options. J Clin Endocrinol Metab *106*, 1-15.
860 10.1210/clinem/dgaa764.
861 11. Randolph, J.F., Jr., Zheng, H., Sowers, M.R., Crandall, C., Crawford, S., Gold, E.B., and
862 Vuga, M. (2011). Change in follicle-stimulating hormone and estradiol across the
863 menopausal transition: effect of age at the final menstrual period. J Clin Endocrinol
864 Metab *96*, 746-754. 10.1210/jc.2010-1746.
865 12. Kelsey, T.W., Wright, P., Nelson, S.M., Anderson, R.A., and Wallace, W.H. (2011). A
866 validated model of serum anti-mullerian hormone from conception to menopause. PLoS
867 One *6*, e22024. 10.1371/journal.pone.0022024.
868 13. Weiss, G., Skurnick, J.H., Goldsmith, L.T., Santoro, N.F., and Park, S.J. (2004). Menopause
869 and hypothalamic-pituitary sensitivity to estrogen. JAMA *292*, 2991-2996.
870 10.1001/jama.292.24.2991.

871 14. Xiong, J., Kang, S.S., Wang, Z., Liu, X., Kuo, T.C., Korkmaz, F., Padilla, A., Miyashita, S.,
872 Chan, P., Zhang, Z., et al. (2022). FSH blockade improves cognition in mice with
873 Alzheimer's disease. Nature *603*, 470-476. 10.1038/s41586-022-04463-0.
874 15. Mao, L., Wang, L., Bennett, S., Xu, J., and Zou, J. (2022). Effects of follicle-stimulating
875 hormone on fat metabolism and cognitive impairment in women during menopause.
876 Front Physiol *13*, 1043237. 10.3389/fphys.2022.1043237.
877 16. Xiong, J., Kang, S.S., Wang, M., Wang, Z., Xia, Y., Liao, J., Liu, X., Yu, S.P., Zhang, Z., Ryu, V.,
878 et al. (2023). FSH and ApoE4 contribute to Alzheimer's disease-like pathogenesis via
879 C/EBPbeta/delta-secretase in female mice. Nat Commun *14*, 6577. 10.1038/s41467-023-
880 42282-7.
881 17. Luckey, T.D. (1972). Introduction to intestinal microecology. Am J Clin Nutr *25*, 1292-1294.
882 10.1093/ajcn/25.12.1292.
883 18. Savage, D.C. (1977). Microbial ecology of the gastrointestinal tract. Annu Rev Microbiol
884 *31*, 107-133. 10.1146/annurev.mi.31.100177.000543.
885 19. Sender, R., Fuchs, S., and Milo, R. (2016). Are We Really Vastly Outnumbered? Revisiting
886 the Ratio of Bacterial to Host Cells in Humans. Cell *164*, 337-340.
887 10.1016/j.cell.2016.01.013.
888 20. Biagi, E., Candela, M., Turroni, S., Garagnani, P., Franceschi, C., and Brigidi, P. (2013).
889 Ageing and gut microbes: perspectives for health maintenance and longevity. Pharmacol
890 Res *69*, 11-20. 10.1016/j.phrs.2012.10.005.

891 21. Zapata, H.J., and Quagliarello, V.J. (2015). The microbiota and microbiome in aging:
892 potential implications in health and age-related diseases. J Am Geriatr Soc *63*, 776-781.
893 10.1111/jgs.13310.
894 22. Parker, A., Romano, S., Ansorge, R., Aboelnour, A., Le Gall, G., Savva, G.M., Pontifex, M.G.,
895 Telatin, A., Baker, D., Jones, E., et al. (2022). Fecal microbiota transfer between young
896 and aged mice reverses hallmarks of the aging gut, eye, and brain. Microbiome *10*, 68.
897 10.1186/s40168-022-01243-w.
898 23. Kundu, P., Lee, H.U., Garcia-Perez, I., Tay, E.X.Y., Kim, H., Faylon, L.E., Martin, K.A.,
899 Purbojati, R., Drautz-Moses, D.I., Ghosh, S., et al. (2019). Neurogenesis and prolongevity
900 signaling in young germ-free mice transplanted with the gut microbiota of old mice. Sci
901 Transl Med *11*. 10.1126/scitranslmed.aau4760.
902 24. Wu, J., Zhuo, Y., Liu, Y., Chen, Y., Ning, Y., and Yao, J. (2021). Association between
903 premature ovarian insufficiency and gut microbiota. BMC Pregnancy Childbirth *21*, 418.
904 10.1186/s12884-021-03855-w.
905 25. Qi, X., Yun, C., Sun, L., Xia, J., Wu, Q., Wang, Y., Wang, L., Zhang, Y., Liang, X., Wang, L., et
906 al. (2019). Gut microbiota-bile acid-interleukin-22 axis orchestrates polycystic ovary
907 syndrome. Nat Med *25*, 1225-1233. 10.1038/s41591-019-0509-0.
908 26. Weger, B.D., Gobet, C., Yeung, J., Martin, E., Jimenez, S., Betrisey, B., Foata, F., Berger, B.,
909 Balvay, A., Foussier, A., et al. (2019). The Mouse Microbiome Is Required for Sex-Specific
910 Diurnal Rhythms of Gene Expression and Metabolism. Cell Metab *29*, 362-382 e368.
911 10.1016/j.cmet.2018.09.023.

912 27. Lombardi, P., Goldin, B., Boutin, E., and Gorbach, S.L. (1978). Metabolism of androgens
913 and estrogens by human fecal microorganisms. J Steroid Biochem *9*, 795-801.
914 10.1016/0022-4731(78)90203-0.
915 28. Adlercreutz, H., Martin, F., Jarvenpaa, P., and Fotsis, T. (1979). Steroid absorption and
916 enterohepatic recycling. Contraception *20*, 201-223. 10.1016/0010-7824(79)90094-5.
917 29. Eriksson, H., and Gustafsson, J.A. (1970). Steroids in germfree and conventional rats.
918 Distribution and excretion of labelled pregnenolone and corticosterone in male and
919 female rats. Eur J Biochem *15*, 132-139. 10.1111/j.1432-1033.1970.tb00987.x.
920 30. Finch, C.E. (2014). The menopause and aging, a comparative perspective. J Steroid
921 Biochem Mol Biol *142*, 132-141. 10.1016/j.jsbmb.2013.03.010.
922 31. Whitehead, J.C., Hildebrand, B.A., Sun, M., Rockwood, M.R., Rose, R.A., Rockwood, K.,
923 and Howlett, S.E. (2014). A clinical frailty index in aging mice: comparisons with frailty
924 index data in humans. J Gerontol A Biol Sci Med Sci *69*, 621-632. 10.1093/gerona/glt136.
925 32. Felicio, L.S., Nelson, J.F., and Finch, C.E. (1986). Prolongation and cessation of estrous
926 cycles in aging C57BL/6J mice are differentially regulated events. Biol Reprod *34*, 849-
927 858. 10.1095/biolreprod34.5.849.
928 33. Johnson, J.S., Spakowicz, D.J., Hong, B.Y., Petersen, L.M., Demkowicz, P., Chen, L., Leopold,
929 S.R., Hanson, B.M., Agresta, H.O., Gerstein, M., et al. (2019). Evaluation of 16S rRNA
930 gene sequencing for species and strain-level microbiome analysis. Nat Commun *10*, 5029.
931 10.1038/s41467-019-13036-1.
932 34. Gupta, S., Mortensen, M.S., Schjorring, S., Trivedi, U., Vestergaard, G., Stokholm, J.,
933 Bisgaard, H., Krogfelt, K.A., and Sorensen, S.J. (2019). Amplicon sequencing provides

934 more accurate microbiome information in healthy children compared to culturing.
935 Commun Biol *2*, 291. 10.1038/s42003-019-0540-1.
936 35. Knight, R., Vrbanac, A., Taylor, B.C., Aksenov, A., Callewaert, C., Debelius, J., Gonzalez, A.,
937 Kosciolek, T., McCall, L.I., McDonald, D., et al. (2018). Best practices for analysing
938 microbiomes. Nat Rev Microbiol *16*, 410-422. 10.1038/s41579-018-0029-9.
939 36. Willis, A.D. (2019). Rarefaction, Alpha Diversity, and Statistics. Front Microbiol *10*, 2407.
940 10.3389/fmicb.2019.02407.
941 37. Hopkins, M.J., Sharp, R., and Macfarlane, G.T. (2002). Variation in human intestinal
942 microbiota with age. Dig Liver Dis *34 Suppl 2*, S12-18. 10.1016/s1590-8658(02)80157-8.
943 38. Yatsunenko, T., Rey, F.E., Manary, M.J., Trehan, I., Dominguez-Bello, M.G., Contreras, M.,
944 Magris, M., Hidalgo, G., Baldassano, R.N., Anokhin, A.P., et al. (2012). Human gut
945 microbiome viewed across age and geography. Nature *486*, 222-227.
946 10.1038/nature11053.
947 39. Luo, M., Chen, Y., Pan, X., Chen, H., Fan, L., and Wen, Y. (2023). E. coli Nissle 1917
948 ameliorates mitochondrial injury of granulosa cells in polycystic ovary syndrome through
949 promoting gut immune factor IL-22 via gut microbiota and microbial metabolism. Front
950 Immunol *14*, 1137089. 10.3389/fimmu.2023.1137089.
951 40. Biagi, E., Franceschi, C., Rampelli, S., Severgnini, M., Ostan, R., Turroni, S., Consolandi, C.,
952 Quercia, S., Scurti, M., Monti, D., et al. (2016). Gut Microbiota and Extreme Longevity.
953 Curr Biol *26*, 1480-1485. 10.1016/j.cub.2016.04.016.

954 41. Wang, N., Li, R., Lin, H., Fu, C., Wang, X., Zhang, Y., Su, M., Huang, P., Qian, J., Jiang, F., et
955 al. (2019). Enriched taxa were found among the gut microbiota of centenarians in East
956 China. PLoS One *14*, e0222763. 10.1371/journal.pone.0222763.
957 42. Douglas, G.M., Maffei, V.J., Zaneveld, J.R., Yurgel, S.N., Brown, J.R., Taylor, C.M.,
958 Huttenhower, C., and Langille, M.G.I. (2020). PICRUSt2 for prediction of metagenome
959 functions. Nat Biotechnol *38*, 685-688. 10.1038/s41587-020-0548-6.
960 43. Murali, R., Balasubramaniam, V., Srinivas, S., Sundaram, S., Venkatraman, G., Warrier, S.,
961 Dharmarajan, A., and Gandhirajan, R.K. (2023). Deregulated Metabolic Pathways in
962 Ovarian Cancer: Cause and Consequence. Metabolites *13*. 10.3390/metabo13040560.
963 44. Ji, Z., Shen, Y., Feng, X., Kong, Y., Shao, Y., Meng, J., Zhang, X., and Yang, G. (2020).
964 Deregulation of Lipid Metabolism: The Critical Factors in Ovarian Cancer. Front Oncol *10*,
965 593017. 10.3389/fonc.2020.593017.
966 45. Borman, S.M., Christian, P.J., Sipes, I.G., and Hoyer, P.B. (2000). Ovotoxicity in female
967 Fischer rats and B6 mice induced by low-dose exposure to three polycyclic aromatic
968 hydrocarbons: comparison through calculation of an ovotoxic index. Toxicol Appl
969 Pharmacol *167*, 191-198. 10.1006/taap.2000.9006.
970 46. Van Kempen, T.A., Milner, T.A., and Waters, E.M. (2011). Accelerated ovarian failure: a
971 novel, chemically induced animal model of menopause. Brain Res *1379*, 176-187.
972 10.1016/j.brainres.2010.12.064.
973 47. Mayer, L.P., Devine, P.J., Dyer, C.A., and Hoyer, P.B. (2004). The follicle-deplete mouse
974 ovary produces androgen. Biol Reprod *71*, 130-138. 10.1095/biolreprod.103.016113.

975 48. Boehme, M., Guzzetta, K.E., Bastiaanssen, T.F.S., van de Wouw, M., Moloney, G.M., Gual-
976 Grau, A., Spichak, S., Olavarria-Ramirez, L., Fitzgerald, P., Morillas, E., et al. (2021).
977 Microbiota from young mice counteracts selective age-associated behavioral deficits.
978 Nat Aging *1*, 666-676. 10.1038/s43587-021-00093-9.
979 49. Subramanian, A., Tamayo, P., Mootha, V.K., Mukherjee, S., Ebert, B.L., Gillette, M.A.,
980 Paulovich, A., Pomeroy, S.L., Golub, T.R., Lander, E.S., and Mesirov, J.P. (2005). Gene set
981 enrichment analysis: a knowledge-based approach for interpreting genome-wide
982 expression profiles. Proc Natl Acad Sci U S A *102*, 15545-15550.
983 10.1073/pnas.0506580102.
984 50. Morris, M.E., Meinsohn, M.C., Chauvin, M., Saatcioglu, H.D., Kashiwagi, A., Sicher, N.A.,
985 Nguyen, N., Yuan, S., Stavely, R., Hyun, M., et al. (2022). A single-cell atlas of the cycling
986 murine ovary. Elife *11*. 10.7554/eLife.77239.
987 51. Jew, B., Alvarez, M., Rahmani, E., Miao, Z., Ko, A., Garske, K.M., Sul, J.H., Pietilainen, K.H.,
988 Pajukanta, P., and Halperin, E. (2020). Accurate estimation of cell composition in bulk
989 expression through robust integration of single-cell information. Nat Commun *11*, 1971.
990 10.1038/s41467-020-15816-6.
991 52. Newman, A.M., Liu, C.L., Green, M.R., Gentles, A.J., Feng, W., Xu, Y., Hoang, C.D., Diehn,
992 M., and Alizadeh, A.A. (2015). Robust enumeration of cell subsets from tissue expression
993 profiles. Nat Methods *12*, 453-457. 10.1038/nmeth.3337.
994 53. Yevshin, I., Sharipov, R., Valeev, T., Kel, A., and Kolpakov, F. (2017). GTRD: a database of
995 transcription factor binding sites identified by ChIP-seq experiments. Nucleic Acids Res
996 *45*, D61-D67. 10.1093/nar/gkw951.

997 54. Zheng, R., Wan, C., Mei, S., Qin, Q., Wu, Q., Sun, H., Chen, C.H., Brown, M., Zhang, X.,
998 Meyer, C.A., and Liu, X.S. (2019). Cistrome Data Browser: expanded datasets and new
999 tools for gene regulatory analysis. Nucleic Acids Res *47*, D729-D735.
1000 10.1093/nar/gky1094.
1001 55. Mei, S., Qin, Q., Wu, Q., Sun, H., Zheng, R., Zang, C., Zhu, M., Wu, J., Shi, X., Taing, L., et
1002 al. (2017). Cistrome Data Browser: a data portal for ChIP-Seq and chromatin accessibility
1003 data in human and mouse. Nucleic Acids Res *45*, D658-D662. 10.1093/nar/gkw983.
1004 56. Huang, H.Y., Li, S.F., Zhao, Z.H., Liang, Z., Zhang, J., and Ding, Y.R. (2011). Association of
1005 polymorphisms for nuclear receptor coactivator 1 gene with egg production traits in the
1006 maternal line of Shaobo hens. Br Poult Sci *52*, 328-332. 10.1080/00071668.2011.577057.
1007 57. Wang, M., Zhang, Y., Wang, T., Zhang, J., Zhou, Z., Sun, Y., Wang, S., Shi, Y., Luan, X.,
1008 Zhang, Y., et al. (2017). The USP7 Inhibitor P5091 Induces Cell Death in Ovarian Cancers
1009 with Different P53 Status. Cell Physiol Biochem *43*, 1755-1766. 10.1159/000484062.
1010 58. Briley, S.M., Jasti, S., McCracken, J.M., Hornick, J.E., Fegley, B., Pritchard, M.T., and
1011 Duncan, F.E. (2016). Reproductive age-associated fibrosis in the stroma of the
1012 mammalian ovary. Reproduction *152*, 245-260. 10.1530/REP-16-0129.
1013 59. Zhang, Z., Schlamp, F., Huang, L., Clark, H., and Brayboy, L. (2020). Inflammaging is
1014 associated with shifted macrophage ontogeny and polarization in the aging mouse ovary.
1015 Reproduction *159*, 325-337. 10.1530/REP-19-0330.
1016 60. Zhou, Z., Yang, X., Pan, Y., Shang, L., Chen, S., Yang, J., Jin, L., Zhang, F., and Wu, Y. (2021).
1017 Temporal transcriptomic landscape of postnatal mouse ovaries reveals dynamic gene

1018 signatures associated with ovarian aging. Hum Mol Genet *30*, 1941-1954.
1019 10.1093/hmg/ddab163.
1020 61. Yang, Q., Chen, W., Cong, L., Wang, M., Li, H., Wang, H., Luo, X., Zhu, J., Zeng, X., Zhu, Z.,
1021 et al. (2024). NADase CD38 is a key determinant of ovarian aging. Nat Aging *4*, 110-128.
1022 10.1038/s43587-023-00532-9.
1023 62. Saul, D., Kosinsky, R.L., Atkinson, E.J., Doolittle, M.L., Zhang, X., LeBrasseur, N.K., Pignolo,
1024 R.J., Robbins, P.D., Niedernhofer, L.J., Ikeno, Y., et al. (2022). A new gene set identifies
1025 senescent cells and predicts senescence-associated pathways across tissues. Nat
1026 Commun *13*, 4827. 10.1038/s41467-022-32552-1.
1027 63. Mehalko, K., Kim, M., Paye, S., Koh, K., Lu, R.J., and Benayoun, B.A. (2023). Lack of
1028 accelerated ovarian aging in a follicle-stimulating hormone receptor haploinsufficiency
1029 model. Transl Med Aging *7*, 1-8. 10.1016/j.tma.2023.01.001.
1030 64. Wrzosek, L., Ciocan, D., Borentain, P., Spatz, M., Puchois, V., Hugot, C., Ferrere, G.,
1031 Mayeur, C., Perlemuter, G., and Cassard, A.M. (2018). Transplantation of human
1032 microbiota into conventional mice durably reshapes the gut microbiota. Sci Rep *8*, 6854.
1033 10.1038/s41598-018-25300-3.
1034 65. Gong, X., Gutala, R., and Jaiswal, A.K. (2008). Quinone oxidoreductases and vitamin K
1035 metabolism. Vitam Horm *78*, 85-101. 10.1016/S0083-6729(07)00005-2.
1036 66. Stachenfeld, N.S. (2014). Hormonal changes during menopause and the impact on fluid
1037 regulation. Reprod Sci *21*, 555-561. 10.1177/1933719113518992.

1038 67. Liu, T., Bowen, R.L., Wilson, A.C., and Atwood, C.S. (2022). Estropause, Sex Hormones
1039 and Metal Homeostasis in the Mouse Brain. Front Neurol *13*, 841822.
1040 10.3389/fneur.2022.841822.
1041 68. Schele, E., Grahnemo, L., Anesten, F., Hallen, A., Backhed, F., and Jansson, J.O. (2013).
1042 The gut microbiota reduces leptin sensitivity and the expression of the obesity-
1043 suppressing neuropeptides proglucagon (Gcg) and brain-derived neurotrophic factor
1044 (Bdnf) in the central nervous system. Endocrinology *154*, 3643-3651. 10.1210/en.2012-
1045 2151.
1046 69. Fan, K.C., Lin, C.C., Liu, Y.C., Chao, Y.P., Lai, Y.J., Chiu, Y.L., and Chuang, Y.F. (2023). Altered
1047 gut microbiota in older adults with mild cognitive impairment: a case-control study.
1048 Front Aging Neurosci *15*, 1162057. 10.3389/fnagi.2023.1162057.
1049 70. Ellis, J.L., Karl, J.P., Oliverio, A.M., Fu, X., Soares, J.W., Wolfe, B.E., Hernandez, C.J., Mason,
1050 J.B., and Booth, S.L. (2021). Dietary vitamin K is remodeled by gut microbiota and
1051 influences community composition. Gut Microbes *13*, 1-16.
1052 10.1080/19490976.2021.1887721.
1053 71. Tarkesh, F., Namavar Jahromi, B., Hejazi, N., and Tabatabaee, H. (2020). Beneficial health
1054 effects of Menaquinone-7 on body composition, glycemic indices, lipid profile, and
1055 endocrine markers in polycystic ovary syndrome patients. Food Sci Nutr *8*, 5612-5621.
1056 10.1002/fsn3.1837.
1057 72. Sibayama-Imazu, T., Fujisawa, Y., Masuda, Y., Aiuchi, T., Nakajo, S., Itabe, H., and Nakaya,
1058 K. (2008). Induction of apoptosis in PA-1 ovarian cancer cells by vitamin K2 is associated

1059 with an increase in the level of TR3/Nur77 and its accumulation in mitochondria and
1060 nuclei. J Cancer Res Clin Oncol *134*, 803-812. 10.1007/s00432-007-0349-z.
1061 73. Harshman, S.G., and Shea, M.K. (2016). The Role of Vitamin K in Chronic Aging Diseases:
1062 Inflammation, Cardiovascular Disease, and Osteoarthritis. Curr Nutr Rep *5*, 90-98.
1063 10.1007/s13668-016-0162-x.
1064 74. Sampathkumar, N.K., Bravo, J.I., Chen, Y., Danthi, P.S., Donahue, E.K., Lai, R.W., Lu, R.,
1065 Randall, L.T., Vinson, N., and Benayoun, B.A. (2020). Widespread sex dimorphism in
1066 aging and age-related diseases. Hum Genet *139*, 333-356. 10.1007/s00439-019-02082-w.
1067 75. Podcasy, J.L., and Epperson, C.N. (2016). Considering sex and gender in Alzheimer
1068 disease and other dementias. Dialogues Clin Neurosci *18*, 437-446.
1069 10.31887/DCNS.2016.18.4/cepperson.
1070 76. Vina, J., and Lloret, A. (2010). Why women have more Alzheimer's disease than men:
1071 gender and mitochondrial toxicity of amyloid-beta peptide. J Alzheimers Dis *20 Suppl 2*,
1072 S527-533. 10.3233/JAD-2010-100501.
1073 77. Varghese, M., Griffin, C., McKernan, K., Eter, L., Abrishami, S., and Singer, K. (2020).
1074 Female adipose tissue has improved adaptability and metabolic health compared to
1075 males in aged obesity. Aging (Albany NY) *12*, 1725-1746. 10.18632/aging.102709.
1076 78. Austad, S.N., and Fischer, K.E. (2016). Sex Differences in Lifespan. Cell Metab *23*, 1022-
1077 1033. 10.1016/j.cmet.2016.05.019.
1078 79. Lemaitre, J.F., Ronget, V., Tidiere, M., Allaine, D., Berger, V., Cohas, A., Colchero, F., Conde,
1079 D.A., Garratt, M., Liker, A., et al. (2020). Sex differences in adult lifespan and aging rates

1080 of mortality across wild mammals. Proc Natl Acad Sci U S A *117*, 8546-8553.
1081 10.1073/pnas.1911999117.
1082 80. Markle, J.G., Frank, D.N., Mortin-Toth, S., Robertson, C.E., Feazel, L.M., Rolle-Kampczyk,
1083 U., von Bergen, M., McCoy, K.D., Macpherson, A.J., and Danska, J.S. (2013). Sex
1084 differences in the gut microbiome drive hormone-dependent regulation of
1085 autoimmunity. Science *339*, 1084-1088. 10.1126/science.1233521.
1086 81. Steegenga, W.T., Mischke, M., Lute, C., Boekschoten, M.V., Pruis, M.G., Lendvai, A.,
1087 Verkade, H.J., Boekhorst, J., Timmerman, H.M., Plosch, T., and Muller, M. (2014). Sexually
1088 dimorphic characteristics of the small intestine and colon of prepubescent C57BL/6 mice.
1089 Biol Sex Differ *5*, 11. 10.1186/s13293-014-0011-9.
1090 82. Org, E., Mehrabian, M., Parks, B.W., Shipkova, P., Liu, X., Drake, T.A., and Lusis, A.J. (2016).
1091 Sex differences and hormonal effects on gut microbiota composition in mice. Gut
1092 Microbes *7*, 313-322. 10.1080/19490976.2016.1203502.
1093 83. Vemuri, R., Sylvia, K.E., Klein, S.L., Forster, S.C., Plebanski, M., Eri, R., and Flanagan, K.L.
1094 (2019). The microgenderome revealed: sex differences in bidirectional interactions
1095 between the microbiota, hormones, immunity and disease susceptibility. Semin
1096 Immunopathol *41*, 265-275. 10.1007/s00281-018-0716-7.
1097 84. Kaliannan, K., Robertson, R.C., Murphy, K., Stanton, C., Kang, C., Wang, B., Hao, L., Bhan,
1098 A.K., and Kang, J.X. (2018). Estrogen-mediated gut microbiome alterations influence
1099 sexual dimorphism in metabolic syndrome in mice. Microbiome *6*, 205. 10.1186/s40168-
1100 018-0587-0.

1101 85. Hornung, R., Boulesteix, A.L., and Causeur, D. (2016). Combining location-and-scale
1102 batch effect adjustment with data cleaning by latent factor adjustment. BMC
1103 Bioinformatics *17*, 27. 10.1186/s12859-015-0870-z.
1104 86. Karimnezhad, A. (2022). More accurate estimation of cell composition in bulk expression
1105 through robust integration of single-cell information. Bioinform Adv *2*, vbac049.
1106 10.1093/bioadv/vbac049.
1107 87. Signorell, A. https://andrisignorell.github.io/DescTools/.
1108 88. Love, M.I., Huber, W., and Anders, S. (2014). Moderated estimation of fold change and
1109 dispersion for RNA-seq data with DESeq2. Genome Biol *15*, 550. 10.1186/s13059-014-
1110 0550-8.
1111 89. Gordon, A. http://hannonlab.cshl.edu/fastx_toolkit/.
1112 90. Pfister, S., Kuettel, V., Ferrero, E. https://github.com/Novartis/granulator.
1113 91. Heinz, S., Benner, C., Spann, N., Bertolino, E., Lin, Y.C., Laslo, P., Cheng, J.X., Murre, C.,
1114 Singh, H., and Glass, C.K. (2010). Simple combinations of lineage-determining
1115 transcription factors prime cis-regulatory elements required for macrophage and B cell
1116 identities. Mol Cell *38*, 576-589. 10.1016/j.molcel.2010.05.004.
1117 92. Ritchie, M.E., Phipson, B., Wu, D., Hu, Y., Law, C.W., Shi, W., and Smyth, G.K. (2015).
1118 limma powers differential expression analyses for RNA-sequencing and microarray
1119 studies. Nucleic Acids Res *43*, e47. 10.1093/nar/gkv007.
1120 93. Tingley, D., Yamamoto, T., Hirose, K., Keele, L., and Imai, K. (2014). mediation: R Package
1121 for Causal Mediation Analysis. Journal of Statistical Software *59*, 1 - 38.
1122 10.18637/jss.v059.i05.

1123 94. Rohart, F., Gautier, B., Singh, A., and Le Cao, K.A. (2017). mixOmics: An R package for
1124 'omics feature selection and multiple data integration. PLoS Comput Biol *13*, e1005752.
1125 10.1371/journal.pcbi.1005752.
1126 95. Bolyen, E., Rideout, J.R., Dillon, M.R., Bokulich, N.A., Abnet, C.C., Al-Ghalith, G.A.,
1127 Alexander, H., Alm, E.J., Arumugam, M., Asnicar, F., et al. (2019). Reproducible,
1128 interactive, scalable and extensible microbiome data science using QIIME 2. Nat
1129 Biotechnol *37*, 852-857. 10.1038/s41587-019-0209-9.
1130 96. Bisanz, J. https://github.com/jbisanz/qiime2R.
1131 97. Dobin, A., Davis, C.A., Schlesinger, F., Drenkow, J., Zaleski, C., Jha, S., Batut, P., Chaisson,
1132 M., and Gingeras, T.R. (2013). STAR: ultrafast universal RNA-seq aligner. Bioinformatics
1133 *29*, 15-21. 10.1093/bioinformatics/bts635.
1134 98. Leek, J.T., and Storey, J.D. (2007). Capturing heterogeneity in gene expression studies by
1135 surrogate variable analysis. PLoS Genet *3*, 1724-1735. 10.1371/journal.pgen.0030161.
1136 99. Liao, Y., Smyth, G.K., and Shi, W. (2014). featureCounts: an efficient general purpose
1137 program for assigning sequence reads to genomic features. Bioinformatics *30*, 923-930.
1138 10.1093/bioinformatics/btt656.
1139 100. Krueger, F. https://www.bioinformatics.babraham.ac.uk/projects/trim_galore/.
1140 101. Callahan, B.J., McMurdie, P.J., Rosen, M.J., Han, A.W., Johnson, A.J., and Holmes, S.P.
1141 (2016). DADA2: High-resolution sample inference from Illumina amplicon data. Nat
1142 Methods *13*, 581-583. 10.1038/nmeth.3869.
1143 102. Wang, Y., and LeCao, K.A. (2020). Managing batch effects in microbiome data. Brief
1144 Bioinform *21*, 1954-1970. 10.1093/bib/bbz105.

1145 103. Fernandes, A.D., Reid, J.N., Macklaim, J.M., McMurrough, T.A., Edgell, D.R., and Gloor,
1146 G.B. (2014). Unifying the analysis of high-throughput sequencing datasets: characterizing
1147 RNA-seq, 16S rRNA gene sequencing and selective growth experiments by compositional
1148 data analysis. Microbiome *2*, 15. 10.1186/2049-2618-2-15.
1149 104. Yilmaz, P., Parfrey, L.W., Yarza, P., Gerken, J., Pruesse, E., Quast, C., Schweer, T., Peplies, J.,
1150 Ludwig, W., and Glockner, F.O. (2014). The SILVA and "All-species Living Tree Project
1151 (LTP)" taxonomic frameworks. Nucleic Acids Res *42*, D643-648. 10.1093/nar/gkt1209.
1152 105. Liberzon, A., Birger, C., Thorvaldsdottir, H., Ghandi, M., Mesirov, J.P., and Tamayo, P.
1153 (2015). The Molecular Signatures Database (MSigDB) hallmark gene set collection. Cell
1154 Syst *1*, 417-425. 10.1016/j.cels.2015.12.004.
1155 106. Gong, T., and Szustakowski, J.D. (2013). DeconRNASeq: a statistical framework for
1156 deconvolution of heterogeneous tissue samples based on mRNA-Seq data.
1157 Bioinformatics *29*, 1083-1085. 10.1093/bioinformatics/btt090.
1158 107. Karl, J.P., Fu, X., Dolnikowski, G.G., Saltzman, E., and Booth, S.L. (2014). Quantification of
1159 phylloquinone and menaquinones in feces, serum, and food by high-performance liquid
1160 chromatography-mass spectrometry. J Chromatogr B Analyt Technol Biomed Life Sci *963*,
1161 128-133. 10.1016/j.jchromb.2014.05.056.
1162

Figure 1

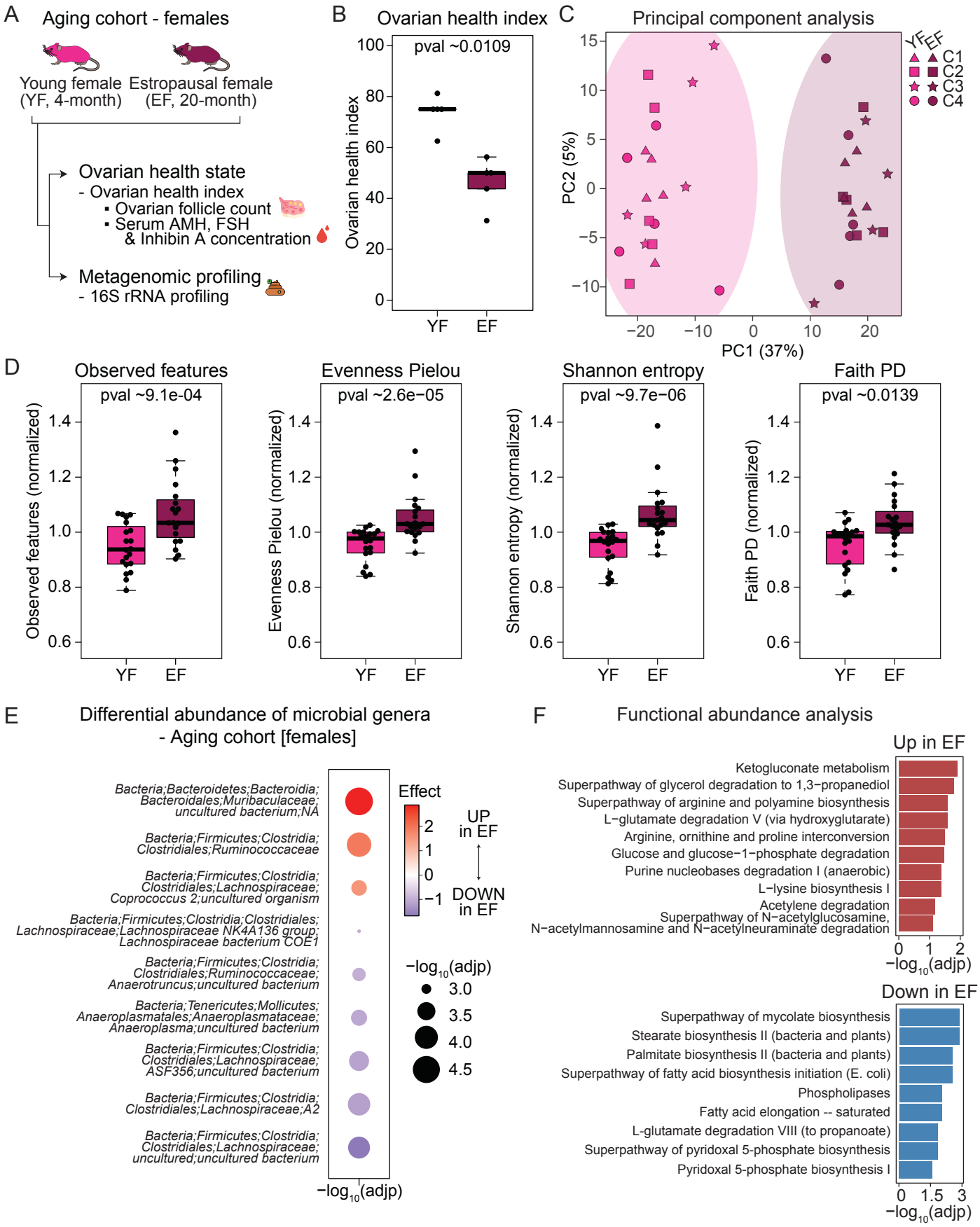
A
Aging cohort - females
Young female (YF, 4-month)
Estropausal female (EF, 20-month)
Ovarian health state
- Ovarian health index
▪ Ovarian follicle count
▪ Serum AMH, FSH & Inhibin A concentration
Metagenomic profiling
- 16S rRNA profiling
B
Ovarian health index
pval ~0.0109
Ovarian health index
YF
EF
C
Principal component analysis
PC2 (5%)
PC1 (37%)
YF
EF
C1
C2
C3
C4
D
Observed features
pval ~9.1e-04
Observed features (normalized)
Evenness Pielou
pval ~2.6e−05
Evenness Pielou (normalized)
Shannon entropy
pval ~9.7e−06
Shannon entropy (normalized)
Faith PD
pval ~0.0139
Faith PD (normalized)
YF
EF
E
Differential abundance of microbial genera
- Aging cohort [females]
Bacteria;Bacteroidetes;Bacteroidia;Bacteroidales;Muribaculaceae;uncultured bacterium;NA
Bacteria;Firmicutes;Clostridia;Clostridiales;Ruminococcaceae
Bacteria;Firmicutes;Clostridia;Clostridiales;Lachnospiraceae;Coprococcus 2;uncultured organism
Bacteria;Firmicutes;Clostridia;Clostridiales;Lachnospiraceae;Lachnospiraceae NK4A136 group;Lachnospiraceae bacterium COE1
Bacteria;Firmicutes;Clostridia;Clostridiales;Ruminococcaceae;Anaerotruncus;uncultured bacterium
Bacteria;Tenericutes;Mollicutes;Anaeroplasmatales;Anaeroplasmataceae;Anaeroplasma;uncultured bacterium
Bacteria;Firmicutes;Clostridia;Clostridiales;Lachnospiraceae;ASF356;uncultured bacterium
Bacteria;Firmicutes;Clostridia;Clostridiales;Lachnospiraceae;A2
Bacteria;Firmicutes;Clostridia;Clostridiales;Lachnospiraceae;uncultured;uncultured bacterium
Effect
UP in EF
DOWN in EF
−log10(adjp)
−log10(adjp)
F
Functional abundance analysis
Up in EF
Ketogluconate metabolism
Superpathway of glycerol degradation to 1,3−propanediol
Superpathway of arginine and polyamine biosynthesis
L−glutamate degradation V (via hydroxyglutarate)
Arginine, ornithine and proline interconversion
Glucose and glucose−1−phosphate degradation
Purine nucleobases degradation I (anaerobic)
L−lysine biosynthesis I
Acetylene degradation
Superpathway of N−acetylglucosamine, N−acetylmannosamine and N−acetylneuraminate degradation
−log10(adjp)
Down in EF
Superpathway of mycolate biosynthesis
Stearate biosynthesis II (bacteria and plants)
Palmitate biosynthesis II (bacteria and plants)
Superpathway of fatty acid biosynthesis initiation (E. coli)
Phospholipases
Fatty acid elongation -- saturated
L-glutamate degradation VIII (to propanoate)
Superpathway of pyridoxal 5-phosphate biosynthesis
Pyridoxal 5-phosphate biosynthesis I
−log10(adjp)

Figure 2

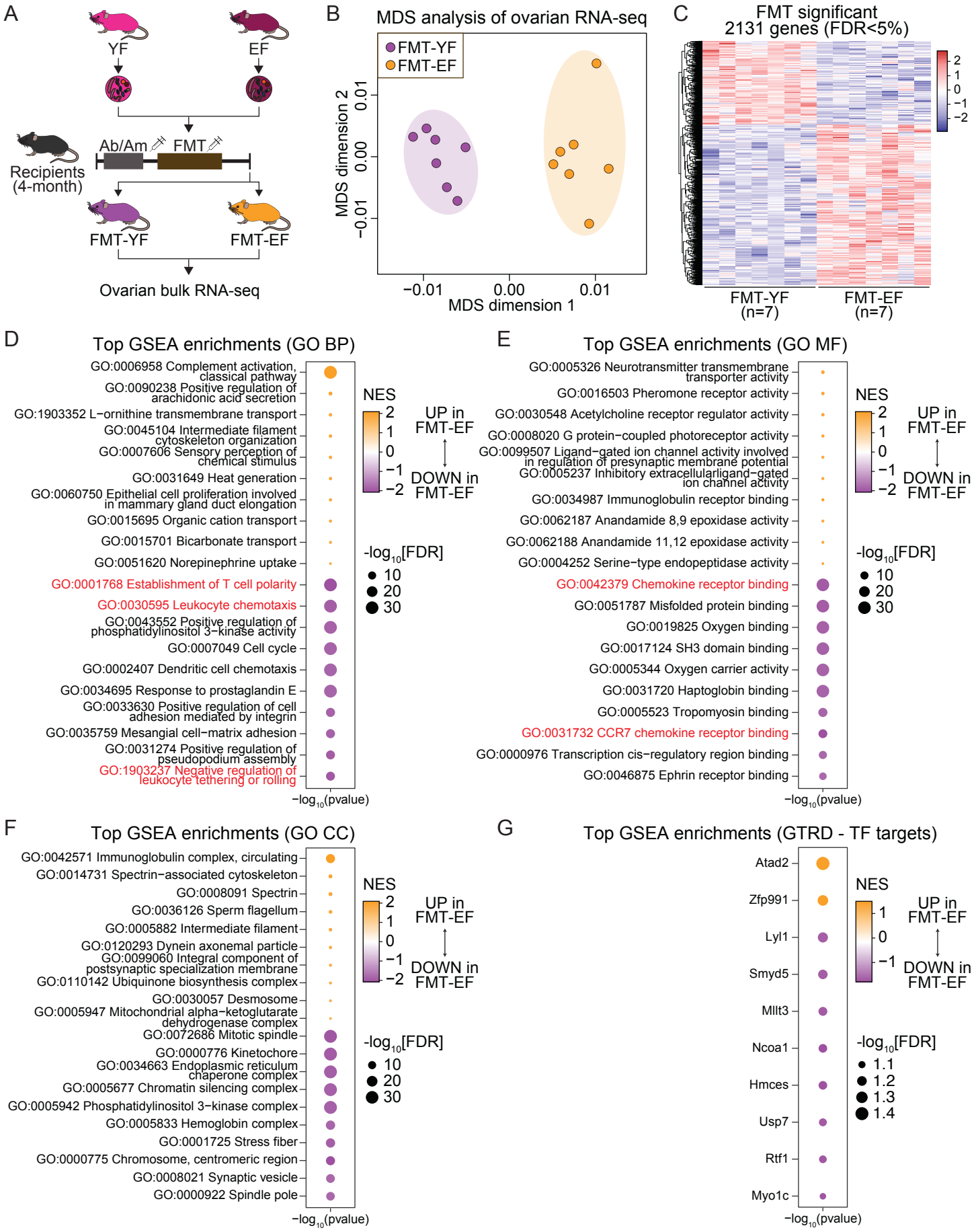
A
YF
EF
Ab/Am
FMT
Recipients
(4-month)
FMT-YF
FMT-EF
Ovarian bulk RNA-seq
B
MDS analysis of ovarian RNA-seq
FMT-YF
FMT-EF
MDS dimension 2
MDS dimension 1
−0.01
0.00
0.01
C
FMT significant
2131 genes (FDR<5%)
FMT-YF
(n=7)
FMT-EF
(n=7)
D
Top GSEA enrichments (GO BP)
GO:0006958 Complement activation, classical pathway
GO:0090238 Positive regulation of arachidonic acid secretion
GO:1903352 L−ornithine transmembrane transport
GO:0045104 Intermediate filament cytoskeleton organization
GO:0007606 Sensory perception of chemical stimulus
GO:0031649 Heat generation
GO:0060750 Epithelial cell proliferation involved in mammary gland duct elongation
GO:0015695 Organic cation transport
GO:0015701 Bicarbonate transport
GO:0051620 Norepinephrine uptake
GO:0001768 Establishment of T cell polarity
GO:0030595 Leukocyte chemotaxis
GO:0043552 Positive regulation of phosphatidylinositol 3−kinase activity
GO:0007049 Cell cycle
GO:0002407 Dendritic cell chemotaxis
GO:0034695 Response to prostaglandin E
GO:0033630 Positive regulation of cell adhesion mediated by integrin
GO:0035759 Mesangial cell−matrix adhesion
GO:0031274 Positive regulation of pseudopodium assembly
GO:1903237 Negative regulation of leukocyte tethering or rolling
−log10(pvalue)
NES
UP in FMT-EF
DOWN in FMT-EF
-log10[FDR]
E
Top GSEA enrichments (GO MF)
GO:0005326 Neurotransmitter transmembrane transporter activity
GO:0016503 Pheromone receptor activity
GO:0030548 Acetylcholine receptor regulator activity
GO:0008020 G protein−coupled photoreceptor activity
GO:0099507 Ligand−gated ion channel activity involved in regulation of presynaptic membrane potential
GO:0005237 Inhibitory extracellularligand−gated ion channel activity
GO:0034987 Immunoglobulin receptor binding
GO:0062187 Anandamide 8,9 epoxidase activity
GO:0062188 Anandamide 11,12 epoxidase activity
GO:0004252 Serine−type endopeptidase activity
GO:0042379 Chemokine receptor binding
GO:0051787 Misfolded protein binding
GO:0019825 Oxygen binding
GO:0017124 SH3 domain binding
GO:0005344 Oxygen carrier activity
GO:0031720 Haptoglobin binding
GO:0005523 Tropomyosin binding
GO:0031732 CCR7 chemokine receptor binding
GO:0000976 Transcription cis−regulatory region binding
GO:0046875 Ephrin receptor binding
F
Top GSEA enrichments (GO CC)
GO:0042571 Immunoglobulin complex, circulating
GO:0014731 Spectrin−associated cytoskeleton
GO:0008091 Spectrin
GO:0036126 Sperm flagellum
GO:0005882 Intermediate filament
GO:0120293 Dynein axonemal particle
GO:0099060 Integral component of postsynaptic specialization membrane
GO:0110142 Ubiquinone biosynthesis complex
GO:0030057 Desmosome
GO:0005947 Mitochondrial alpha−ketoglutarate dehydrogenase complex
GO:0072686 Mitotic spindle
GO:0000776 Kinetochore
GO:0034663 Endoplasmic reticulum chaperone complex
GO:0005677 Chromatin silencing complex
GO:0005942 Phosphatidylinositol 3−kinase complex
GO:0005833 Hemoglobin complex
GO:0001725 Stress fiber
GO:0000775 Chromosome, centromeric region
GO:0008021 Synaptic vesicle
GO:0000922 Spindle pole
G
Top GSEA enrichments (GTRD - TF targets)
Atad2
Zfp991
Lyl1
Smyd5
Mllt3
Ncoa1
Hmces
Usp7
Rtf1
Myo1c

Figure 3

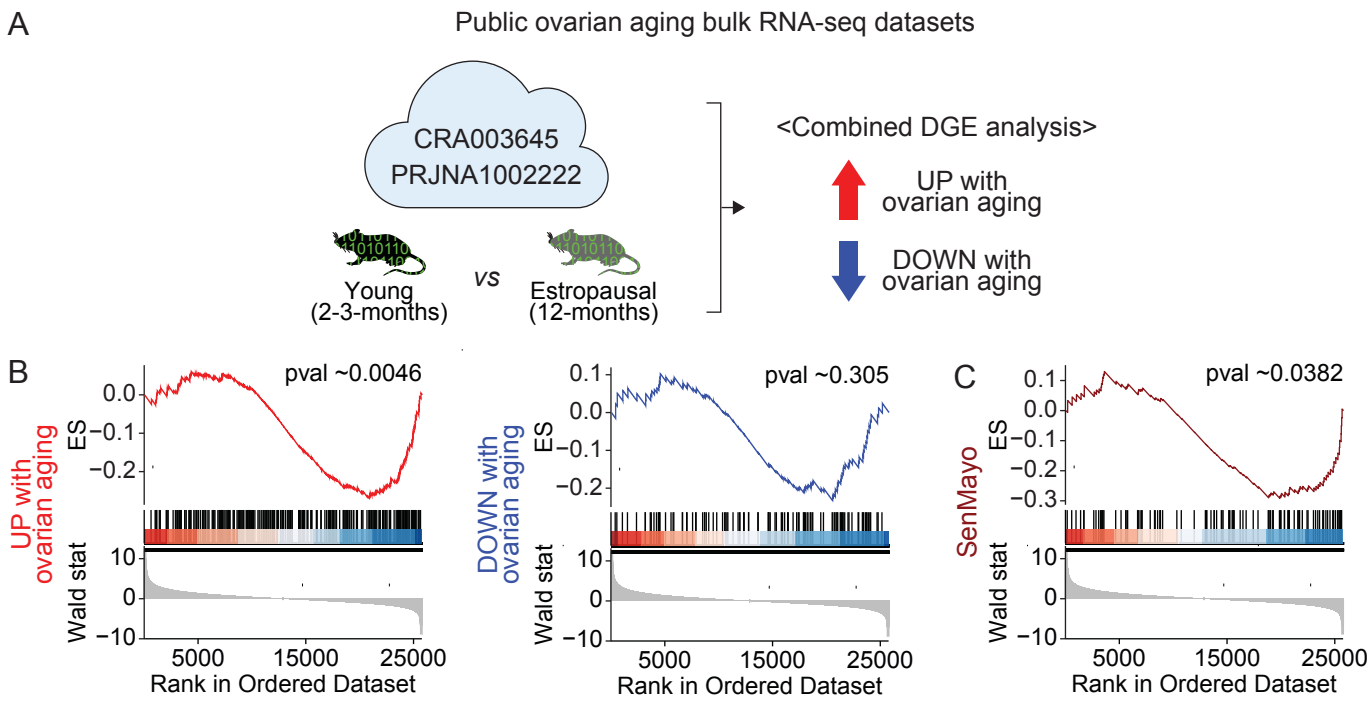
A
Public ovarian aging bulk RNA-seq datasets
CRA003645
PRJNA1002222
Young
(2-3-months)
vs
Estropausal
(12-months)
<Combined DGE analysis>
UP with
ovarian aging
DOWN with
ovarian aging
B
pval ~0.0046
UP with
ovarian aging
ES
Wald stat
Rank in Ordered Dataset
pval ~0.305
DOWN with
ovarian aging
C
pval ~0.0382
SenMayo

Figure 4

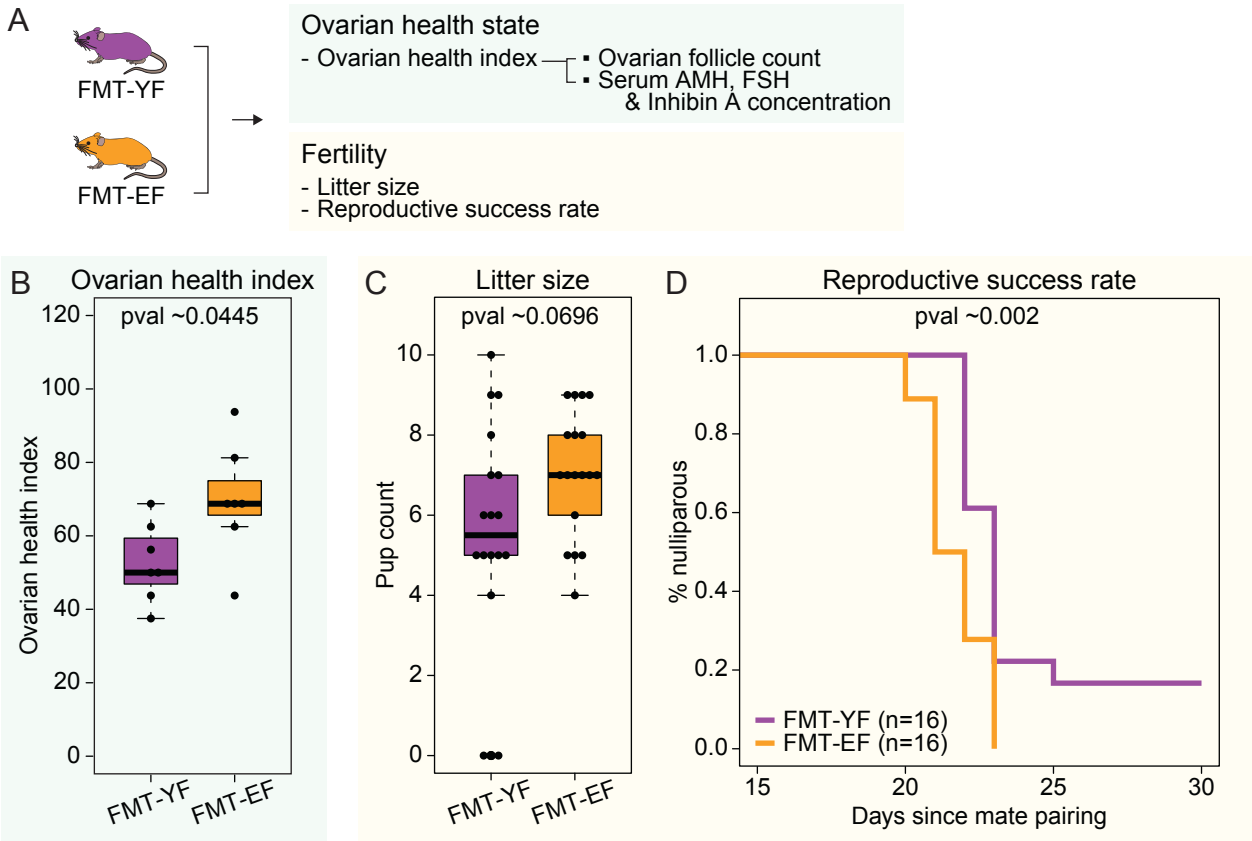
A
FMT-YF
FMT-EF
Ovarian health state
- Ovarian health index
▪ Ovarian follicle count
▪ Serum AMH, FSH & Inhibin A concentration
Fertility
- Litter size
- Reproductive success rate
B
Ovarian health index
pval ~0.0445
Ovarian health index
120
100
80
60
40
20
0
FMT-YF
FMT-EF
C
Litter size
pval ~0.0696
Pup count
10
8
6
4
2
0
FMT-YF
FMT-EF
D
Reproductive success rate
pval ~0.002
% nulliparous
1.0
0.8
0.6
0.4
0.2
0.0
FMT-YF (n=16)
FMT-EF (n=16)
15
20
25
30
Days since mate pairing

Figure 5

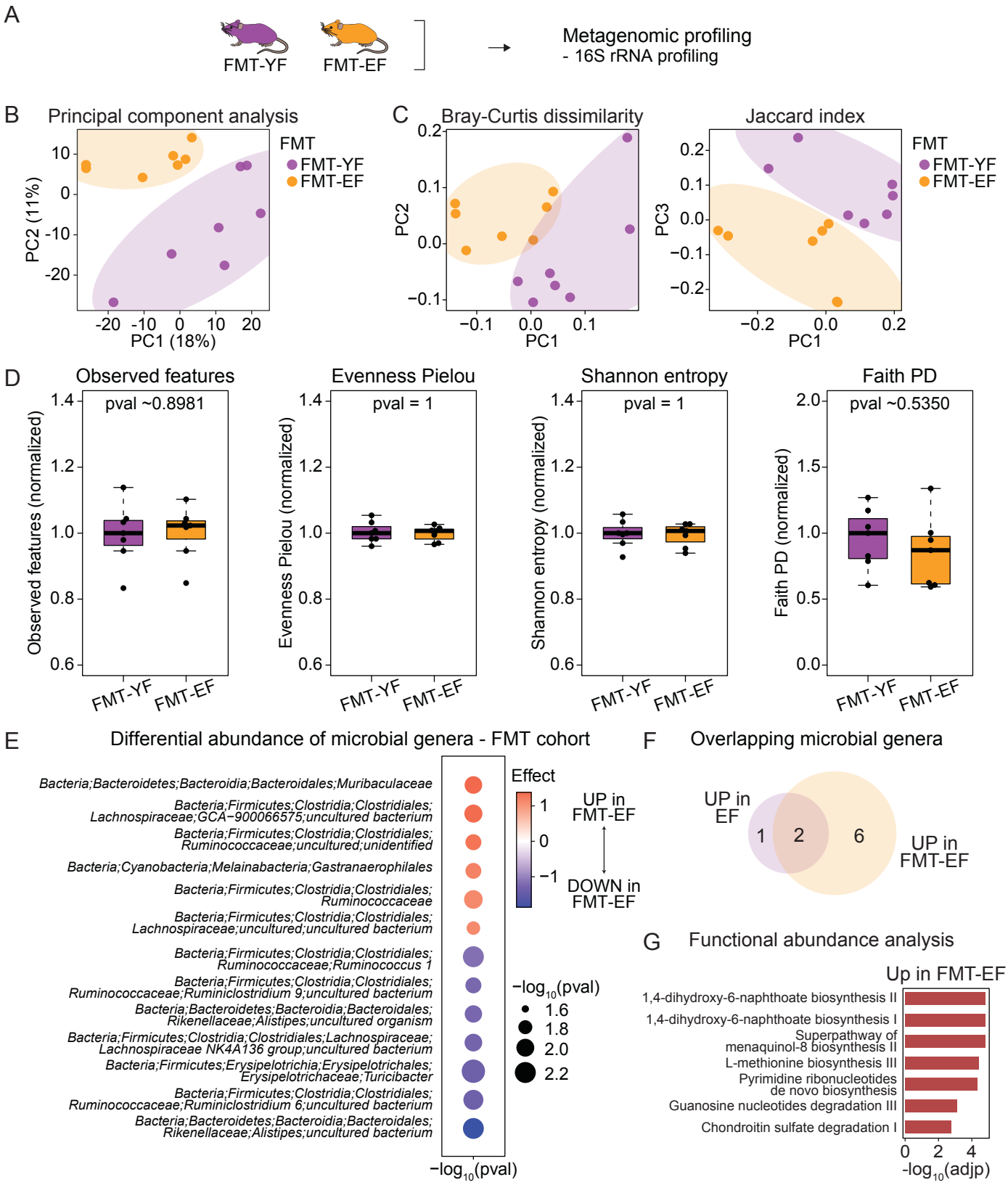
A
FMT-YF
FMT-EF
Metagenomic profiling
- 16S rRNA profiling
B
Principal component analysis
FMT
FMT-YF
FMT-EF
PC2 (11%)
PC1 (18%)
C
Bray-Curtis dissimilarity
Jaccard index
PC2
PC3
PC1
D
Observed features
Evenness Pielou
Shannon entropy
Faith PD
pval ~0.8981
pval = 1
pval = 1
pval ~0.5350
Observed features (normalized)
Evenness Pielou (normalized)
Shannon entropy (normalized)
Faith PD (normalized)
E
Differential abundance of microbial genera - FMT cohort
Bacteria;Bacteroidetes;Bacteroidia;Bacteroidales;Muribaculaceae
Bacteria;Firmicutes;Clostridia;Clostridiales;Lachnospiraceae;GCA−900066575;uncultured bacterium
Bacteria;Firmicutes;Clostridia;Clostridiales;Ruminococcaceae;uncultured;unidentified
Bacteria;Cyanobacteria;Melainabacteria;Gastranaerophilales
Bacteria;Firmicutes;Clostridia;Clostridiales;Ruminococcaceae
Bacteria;Firmicutes;Clostridia;Clostridiales;Lachnospiraceae;uncultured;uncultured bacterium
Bacteria;Firmicutes;Clostridia;Clostridiales;Ruminococcaceae;Ruminococcus 1
Bacteria;Firmicutes;Clostridia;Clostridiales;Ruminococcaceae;Ruminiclostridium 9;uncultured bacterium
Bacteria;Bacteroidetes;Bacteroidia;Bacteroidales;Rikenellaceae;Alistipes;uncultured organism
Bacteria;Firmicutes;Clostridia;Clostridiales;Lachnospiraceae;Lachnospiraceae NK4A136 group;uncultured bacterium
Bacteria;Firmicutes;Erysipelotrichia;Erysipelotrichales;Erysipelotrichaceae;Turicibacter
Bacteria;Firmicutes;Clostridia;Clostridiales;Ruminococcaceae;Ruminiclostridium 6;uncultured bacterium
Bacteria;Bacteroidetes;Bacteroidia;Bacteroidales;Rikenellaceae;Alistipes;uncultured bacterium
Effect
UP in FMT-EF
DOWN in FMT-EF
−log10(pval)
−log10(pval)
F
Overlapping microbial genera
UP in EF
UP in FMT-EF
1
2
6
G
Functional abundance analysis
Up in FMT-EF
1,4-dihydroxy-6-naphthoate biosynthesis II
1,4-dihydroxy-6-naphthoate biosynthesis I
Superpathway of menaquinol-8 biosynthesis II
L-methionine biosynthesis III
Pyrimidine ribonucleotides de novo biosynthesis
Guanosine nucleotides degradation III
Chondroitin sulfate degradation I
-log10(adjp)

Figure 6

A

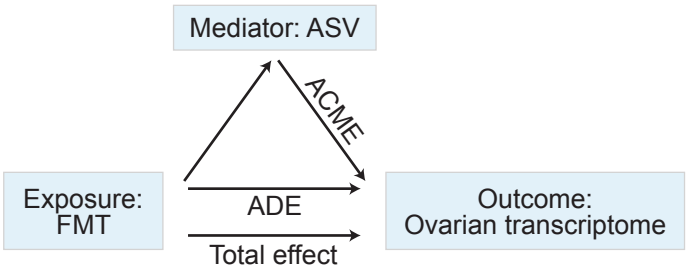
Mediator: ASV
ACME
Exposure:
FMT
ADE
Outcome:
Ovarian transcriptome
Total effect

B

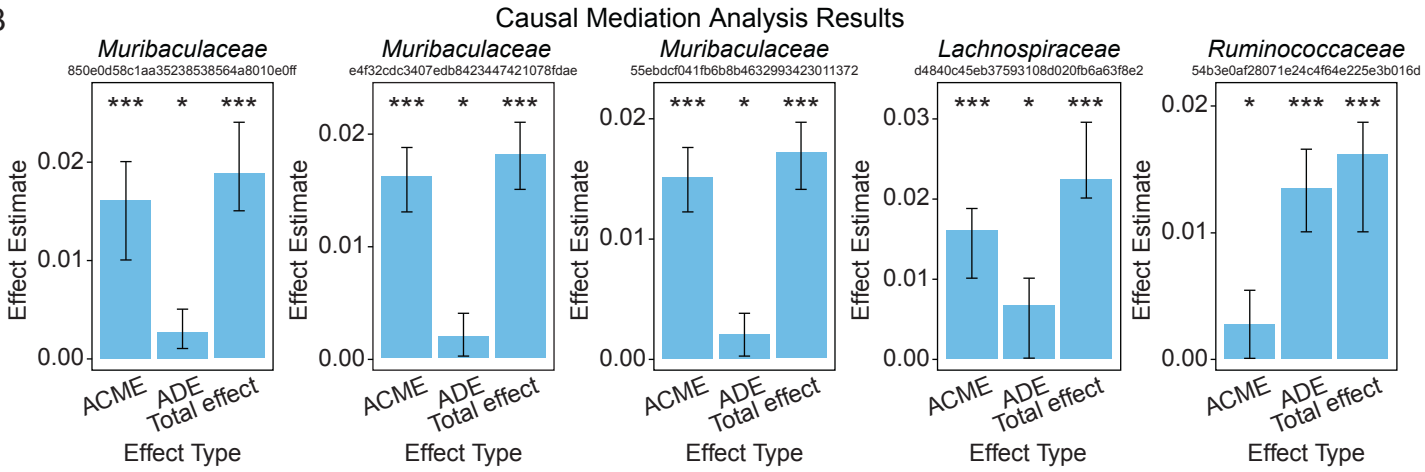
Causal Mediation Analysis Results
Muribaculaceae
850e0d58c1aa35238538564a8010e0ff
Muribaculaceae
e4f32cdc3407edb8423447421078fdae
Muribaculaceae
55ebdcf041fb6b8b4632993423011372
Lachnospiraceae
d4840c45eb37593108d020fb6a63f8e2
Ruminococcaceae
54b3e0af28071e24c4f64e225e3b016d
Effect Estimate
Effect Type
ACME
ADE
Total effect
***
*